CMI

www.nature.com/cmi

ARTICLE

Check for updates

Metabolic reprogramming by Syntenin-1 directs RA FLS and endothelial cell-mediated inflammation and angiogenesis

Anja Meyer[1,2], Stephanie R. Zack[1,2], Wes Nijim[2], Adel Burgos[1,2], Vishwa Patel[2], Brian Zanotti[3], Michael V. Volin[3], M. Asif Amin[4], Myles J. Lewis[5,6], Costantino Pitzalis[5,6,7], Shiva Arami[2], Joseph A. Karam[8], Nadera J. Sweiss[2] and Shiva Shahrara[1,2]✉

A novel rheumatoid arthritis (RA) synovial fluid protein, Syntenin-1, and its receptor, Syndecan-1 (SDC-1), are colocalized on RA synovial tissue endothelial cells and fibroblast-like synoviocytes (FLS). Syntenin-1 exacerbates the inflammatory landscape of endothelial cells and RA FLS by upregulating transcription of IRF1/5/7/9, IL-1β, IL-6, and CCL2 through SDC-1 ligation and HIF1α, or mTOR activation. Mechanistically, Syntenin-1 orchestrates RA FLS and endothelial cell invasion via SDC-1 and/or mTOR signaling. In Syntenin-1 reprogrammed endothelial cells, the dynamic expression of metabolic intermediates coincides with escalated glycolysis along with unchanged oxidative factors, AMPK, PGC-1α, citrate, and inactive oxidative phosphorylation. Conversely, RA FLS rewired by Syntenin-1 displayed a modest glycolytic-ATP accompanied by a robust mitochondrial-ATP capacity. The enriched mitochondrial-ATP detected in Syntenin-1 reprogrammed RA FLS was coupled with mitochondrial fusion and fission recapitulated by escalated Mitofusin-2 and DRP1 expression. We found that VEGFR1/2 and Notch1 networks are responsible for the crosstalk between Syntenin-1 rewired endothelial cells and RA FLS, which are also represented in RA explants. Similar to RA explants, morphological and transcriptome studies authenticated the importance of VEGFR1/2, Notch1, RAPTOR, and HIF1α pathways in Syntenin-1 arthritic mice and their obstruction in SDC-1 deficient animals. Consistently, dysregulation of SDC-1, mTOR, and HIF1α negated Syntenin-1 inflammatory phenotype in RA explants, while inhibition of HIF1α impaired synovial angiogenic imprint amplified by Syntenin-1. In conclusion, since the current therapies are ineffective on Syntenin-1 and SDC-1 expression in RA synovial tissue and blood, targeting this pathway and its interconnected metabolic intermediates may provide a novel therapeutic strategy.

Keywords: Syntenin-1; Syndecan-1; RA FLS; RA explants; immunometabolism

Cellular & Molecular Immunology (2024) 21:33–46; https://doi.org/10.1038/s41423-023-01108-8

INTRODUCTION

Melanoma differentiation-associated gene-9 (MDA-9) or Syntenin-1 is a cytosolic adaptor protein that can bind to the intracellular domain of Syndecan-1 (SDC-1, surface heparan sulfate proteoglycan) through its PDZ2 domain activating the phosphorylation of FAK, Src, p38 MAPK, and AKT in melanoma and breast cancer cells [1, 2]. In parallel, Syntenin-1 has other binding partners, including CD63, Merlin, and IL-5R, that bind to its PDZ1 domain [3, 4]. The PDZ1 domain exhibits weak binding to its target proteins, conversely the Syntenin-1-interacting protein, SDC-1 has a stronger binding capacity to the PDZ2 domain [3, 5].

Overexpression of Syntenin-1 in lung cancer tissue and sera was linked to poor prognosis [6], and Syntenin-1 KO mice displayed delayed tumor initiation and mitigated lung metastasis [7]. Consistently, elevated SDC-1 sera in lung [8] or liver [9] cancer patients and its potentiated protein expression in the stroma and tumor cells in gastric and pancreatic cancer [10] correlated with a high risk of recurrence and metastatic potential. In contrast, others report that SDC-1-deficient mice exhibit advanced tumor growth in colitis-induced colon carcinoma because of escalated IL-6 production and STAT3 signaling [11]. Similarly, SDC-1 KO mice subjected to imiquimod-induced psoriasis illustrated accentuated skin inflammation compared to the wild-type (WT) mice in part due to the expansion of Tγδ17 cells [12]. Moreover, SDC-1 KO mice displayed altered metabolism due to glucose intolerance and insulin resistance [13].

Syntenin-1 is enriched in rheumatoid arthritis (RA) relative to osteoarthritis (OA) synovial fluid (SF) [14]. Intriguingly, the expression of Syntenin-1 and SDC-1 is amplified on RA synovial tissue (ST) lining, sublining, and blood vessels compared to normal counterparts, where the ligand and the receptor colocalize [14, 15]. RNAseq analysis revealed that Syntenin-1 and SDC-1 transcriptomes were linked to the number of $CD68^+$ macrophages (MΦs) in RA STs [14, 16]. Interestingly, Syntenin-1 and SDC-1 expression are mutually

[1]Jesse Brown VA Medical Center, Chicago, IL, USA. [2]Department of Medicine, Division of Rheumatology, The University of Illinois at Chicago, Chicago, IL, USA. [3]Department of Microbiology and Immunology, Midwestern University, Downers Grove, IL, USA. [4]Division of Rheumatology and Clinical Autoimmunity Center of Excellence, University of Michigan, Ann Arbor, MI, USA. [5]Centre for Experimental Medicine and Rheumatology, William Harvey Research Institute, Barts and The London School of Medicine and Dentistry, Queen Mary University of London, London, United Kingdom. [6]Centre for Experimental Medicine & Rheumatology, William Harvey Research Institute, Queen Mary University of London and Barts NIHR BRC & NHS Trust, London, UK. [7]Department of Biomedical Sciences, Humanitas University, and Humanitas Research Hospital, Milan, Italy. [8]Department of Orthopedic Surgery, the University of Illinois at Chicago, Chicago, IL, USA. ✉email: shahrara@uic.edu

Received: 19 June 2023 Accepted: 1 November 2023
Published online: 18 December 2023

elevated by LPS/IFNγ stimulation in RA monocyte-differentiated MΦs. The Syntenin-1 transcriptome in RA blood is connected to CCP and bone erosion [14, 16]. Accordingly, SDC-1 expression in RA synovial tissue is implicated in ultrasound (US) ST thickness and radiographic bone erosion [14, 16]. Distinct from these findings, others have shown that SDC-1 transcription levels were downregulated at the erosive site relative to intact osteoclast cartilage [17]. Recapitulating the association of blood Syntenin-1 and synovial SDC-1 with total Sharp x-ray score, RA precursor cells exposed to Syntenin-1 were reconfigured into mature osteoclasts via transcriptional upregulation of RANK, CTSK, and NFATc1 [14, 16].

Earlier studies have unmasked that the pathogenic effect of Syntenin-1 is advanced by reprogramming naïve cells into metabolic RA $CD14^{+}CD86^{+}GLUT1^{+}$ MΦs that can cross-regulate Th1 cells in part through IL-12 and IL-18 induction [14]. Moreover, collagen-induced arthritis (CIA) was mitigated in SDC-1 KO mice due to constrained joint $F480^{+}iNOS^{+}$MΦs frequency and diminished IL-6 and IL-1β transcription compared to wild-type mice [18]. Nevertheless, the molecular mechanism and malfunctioning metabolic machinery of Syntenin-1 and SDC-1 are undefined in endothelial cells, RA fibroblast-like synoviocytes (FLS), and RA explants.

We show for the first time that Syntenin-1 and SDC-1 are colocalized on RA endothelial cells and FLS and cross-link the arthritogenicity of these cells by influencing their inflammatory, angiogenic, and metabolic landscapes. Endothelial cells exposed to Syntenin-1 exhibit an inflammatory and proangiogenic reconfiguration along with escalated glycolysis through SDC-1, RAPTOR, and HIF1α signaling. Uniquely, RA FLS reprogrammed by Syntenin-1 display an inflammatory and oxidative stress phenotype, related to SDC-1 and HIF1α activation that coincides with mitochondrial dysregulation via Mitofusin-2 and DRP1 induction. Nonetheless, the glycolytic profile of RA FLS, reprogrammed by Syntenin-1 is restricted to RAPTOR which can also modulate its migration. The Syntenin-1-induced arthritis model exemplifies Syntenin-1-activated RA explants by highlighting the significance of inflammatory and proangiogenic networks and their connection to SDC-1, RAPTOR, and HIF1α pathways. Importantly, we found that the VEGFR1/2 and Notch1 axes play a critical role in Syntenin-1-induced interplay between endothelial cells and RA FLS which is represented in RA explants. Notably, in RA explants, inhibition of SDC-1, mTOR, and HIF1α, dysregulated the Syntenin-1-enhanced inflammatory remodeling, while HIF1αi was also responsible for disrupting the angiogenic profile. In conclusion, targeting Syntenin-1 and its downstream metabolic pathways may provide a novel strategy for RA therapy.

MATERIALS AND METHODS

Cells

FLS from fresh RA ST were isolated by mincing and digestion in a solution of dispase, collagenase, and DNase. Cells were used between passages 3 and 9 [19–22]. Human umbilical vein endothelial cells (HUVECs) were purchased from Lonza and used between passages 3 and 9 [22–24]. HUVECs were used as surrogates for RA endothelial cells as an adequate number of cells could not be isolated from RA STs.

Rheumatoid Arthritis explants

RA ST (30 mg) was cut into small pieces to allow proper access to stimuli and were starved o/n in 0% FBS RPMI with or without SDC-1 Ab (1:100), mTOR1i (1 μM), and HIF1αi (2 μM). RA STs were stimulated with Syntenin-1 (1000 ng/ml) for 6-8h. Tissues were harvested for transcriptome analysis and supernatants were used for protein quantification by ELISA.

RNAseq and Single-cell RNAseq transcriptome analysis

The web interface https://peac.hpc.qmul.ac.uk/ developed by Lewis et al. [16] was used to evaluate the expression of Syntenin-1 and SDC-1 in synovial tissues and blood from early RA in the PEAC study. The DAS-based European League Against Rheumatism (EULAR) response criteria were generated to quantify individual responses in clinical trials. The EULAR response criteria classify individual patients as non- (ΔDAS28 ≤0.6), moderate (ΔDAS28 ≤1.2 & >0.6), or good responders (ΔDAS28 >1.2). Detailed methods for the generation of data used in this web interface have been published previously [16, 25]. Gene transcript expression levels are expressed as variance stabilizing transformation transformed read counts using the Bioconductor package DESeq2. The raw RNAseq data have been deposited at ArrayExpress accession E-MTAB-6141.

The single-cell RNA sequencing data from Wei et al. [26] was accessed from the Broad Institute Single Cell portal at the following URL: https://singlecell.broadinstitute.org/single_cell/study/SCP469/synovial-fibroblast-positional-identity-controlled-by-inductive-notch-signaling-underlies-pathologic-damage-in-inflammatory-arthritis. A cohort of RA patients that fulfilled the ACR 2010 Rheumatoid Arthritis classification criteria were included. Synovial tissue samples were acquired when the patients underwent either joint replacement or synovectomy procedures.

The RNAseq dataset GSE198520 deposited by Wang et al. [27] was accessed using the web interface https://www.ncbi.nlm.nih.gov/geo/geo2r/?acc=GSE198520/ to evaluate the expression of SDCBP and SDC-1 in RA synovium biopsied from 27 RA patients 12 weeks after treatment with anti-TNF (Certolizumab). Patients in this cohort fulfilled the 2010 ACR/EULAR RA Classification Criteria and were enrolled at the Centre for Experimental Medicine and Rheumatology, Barts and The London School of Medicine, Queen Mary University of London, UK. RA patients exhibited clinically defined synovitis and fit the criteria for UK NICE guidelines (failure of at least 2 csDMARDs and DAS28 ≥ 5.1) to start anti-TNF therapy. Following enrollment, patients underwent minimally invasive US-guided synovial biopsy of the most inflamed joint (ultrasound synovial thickening score ≥ 2). The patient data were grouped and displayed based on whether the patients were considered non-responders, moderate responders, or good responders to anti-TNF therapy. Response to therapy was evaluated using ACR/EULAR DAS28 response criteria defined as good response (ΔDAS [DAS28 at baseline – DAS28 at 12 weeks after treatment] >1.2 with DAS28 at 12 weeks ≤ 3.2), moderate response (DAS28 change >1.2 with DAS28 at 12 weeks >3.2, or DAS28 change between 0.6-1.2 with DAS28 at 12 weeks ≤5.1), or nonresponse (DAS28 ≤0.6, or DAS28 change between 0.6-1.2 with DAS28 at 12 weeks > 5.1) [28]. Data were further separated based on whether the patients were non-responders or responders to anti-TNF (Certolizumab) therapy.

The web interface https://r4ra.hpc.qmul.ac.uk/ developed by Rivellese et al. [29] was used to evaluate the expression of SDCBP and SDC-1 in synovial tissue from RA patients that were treated with rituximab or tocilizumab. A cohort of 164 patients aged 18 years or over who fulfilled the 2010 American College of Rheumatology/European Alliance of Associations for Rheumatology (EULAR) classification for RA and were eligible for treatment with rituximab therapy according to UK NICE guidelines (patients who failed or were intolerant to csDMARD therapy and at least one biologic therapy) were included in the trial. Initially, a synovial biopsy was taken of a clinically active joint at the beginning of the trial. Patients were then randomized to rituximab or tocilizumab treatment administered as either two 1,000 mg intravenous rituximab infusions 2 weeks apart or intravenous tocilizumab at a dose of 8 mg/kg at 4-week intervals. Detailed methods for the generation of data used in this web interface have been published previously [29]. The patient data were grouped based on response to therapy using the ACR/EULAR DAS28 C reactive protein (CRP) response criteria as described above.

Syntenin-1 stimulation and inhibition

HUVECs or RA FLS were either untreated (PBS) or treated with Syntenin-1 (1000 ng/ml, NKMAX) for 6h to 48h. For blocking specific mechanism of action, cells were starved overnight in the presence of 2-deoxy-D-glucose (2-DG; 5 mM, Sigma-Aldrich), hypoxia-inducible factor 1α inhibitor (HIF1αi; 2 μM, Calbiochem), mTOR inhibitor (mTORi; 1 μM; Everolimus, Sigma-Aldrich), cMYCi (50 μM, Sigma-Aldrich), human IL-5R antibody (IL5Ra; 2 μg/ml, R&D Systems), PDZ1 domain inhibitor peptide (PDZ1; 10 μM, Tocris Bioscience), or SDC-1 antibody (SDCab; 1:100, Diaclone) following Syntenin-1 (1000 ng/ml, NKMAX Co.) stimulation for 6h or 24h. Cells were subsequently harvested in TRIzol reagent (Life Technologies) or RIPA buffer (Cell Signaling) for mRNA quantification and western blot analysis; conditioned media was collected for ELISA.

RA FLS and HUVEC scratch assay

A scratch was created in the middle of the wells that contained confluent HUVECs or RA FLS. Thereafter, cells were either untreated (PBS) or treated

with Syntenin-1 (1000 ng/ml), or 10% FBS and bFGF (100 ng/ml) as a positive control for 24h. In parallel, cells were treated with SDC-1 Ab (1:100), IL-5R Ab (2 μg/ml), PDZ1i (10 μM), mTORi (1μM), or HIF1αi (2 μM) for 24h. In all scratch assay experiments, cells were fixed with 10% formalin for 1h at 37 °C and were subsequently stained with 0.05% crystal violet for 1h before imaging. The number of cells in the scratch area was counted and compared to the untreated control.

Animal studies

All animal studies were approved by the University of Illinois at Chicago Animal Care and Use Committee (No. 22-008). Wild-type C57BL/6 mice (≥ 8 weeks old; Jackson Laboratory, Bar Harbor, Maine, USA) were bred in-house. SDC-1$^{-/-}$ mice were generated as previously described and kindly provided by Dr. Caroline Alexander (University of Wisconsin–Madison) [30]. Animals were housed in sterile static micro isolator cages on autoclaved corncob bedding with water bottles in a specific-pathogen-free (SPF) facility. Animal food is irradiated, and water is autoclaved. Both food and water are provided *ad libitum*. The standard photoperiod for rodent rooms is 14 hours of light and 10 hours of darkness. Animals were provided with autoclaved nesting materials. Cages are changed at least weekly in either a biosafety cabinet or a HEPA-filtered animal transfer station. Eight- to twelve-week-old WT and SDC-1$^{-/-}$ mice were injected intra-articularly with adenovirus (ad)-ctrl or ad-Syntenin-1 (3×10^{10} viral particles/ankle, Welgen) on days 0, 7, and 14. Joint circumference was assessed by a caliper and mice were sacrificed on day 15. Ankles were harvested and used for further analysis.

Quantitative Real-Time PCR

According to the manufacturer's instructions, RNA was isolated using a TRIzol reagent (Life Technologies). Transcription to cDNA and subsequent qRT-PCR analysis was performed using the High-Capacity cDNA Reverse Transcription Kit (Applied Biosystems) and TaqMan Gene Expression Master Mix (Applied Biosystems). Predesigned IDT primers or TaqMan gene expression assays were used (Tables 1 and 2). Data are presented as fold change ($2^{-\Delta\Delta Ct}$) normalized to the housekeeping gene (actin) and compared to the control. Data were acquired with the QuantStudio5 (Applied Biosystems) qRT-PCR device.

Western blot analysis

Samples were lysed in RIPA buffer (Cell Signaling Technology) supplemented with protease and phosphatase inhibitors (Roche laboratories) and protein concentration was assessed with the Pierce BCA Protein Assay Kit (ThermoFisher Scientific) following the manufacturer's instructions. Lysates were run on 10% polyacrylamide gels. Blotting was performed with the Trans-Blot Turbo Transfer System (Bio-Rad Laboratories). Samples were

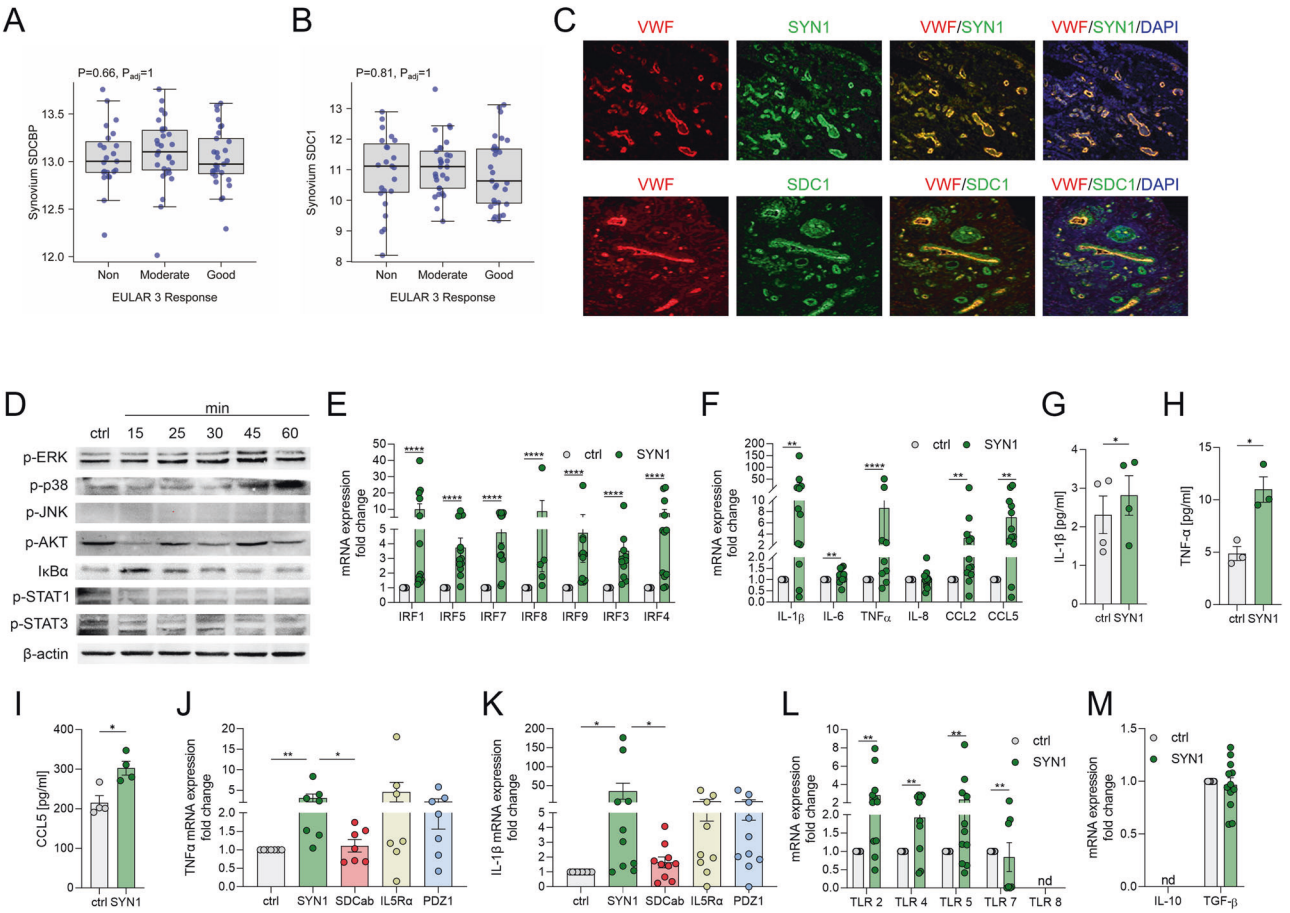

Fig. 1 Syntenin-1 reprogrammed endothelial cells display a robust inflammatory phenotype. **A, B**. Relative expression of Syntenin-1 (**A**) or SDC-1 (**B**) was determined by RNAseq [16] in synovial tissue biopsies from RA non-responsive (ΔDAS28 ≤0.6, $n = 23$), moderate (ΔDAS28 ≤1.2 & >0.6, $n = 29$), and good responsive (ΔDAS28 >1.2, $n = 29$) patients. **C**. RA STs were fluorescently stained to authenticate the colocalization of SDC-1 and Syntenin-1 on VWF^{+}endothelial cells in the presence or absence of DAPI, ($n = 3$, original magnification x 20). **D**. HUVECs were treated with Syntenin-1 (1000 ng/ml) for 0-60 mins and phosphorylation of ERK, p38, JNK, AKT, STAT1, STAT3, and degradation of IκBα was determined by western blot analysis and β-actin served as a loading control, $n = 3$. **E–M**. HUVECs were treated with PBS (ctrl) or Syntenin-1 (1000 ng/ml) in the presence or absence of SDC-1 Ab (SDCab; 1:100), IL-5R Ab (IL5Ra; 2 μg/ml), or PDZ1i (PDZ1; 10 μM) for 6h or 24h and transcription or translation levels of IRFs (**E**), inflammatory mediators (**F**), IL-1β (**G, K**), TNFα (**H, J**), CCL5 (**I**) TLRs (**L**), and pro-repair factors (**M**) was assessed by qRT-PCR and/or ELISA ($n = 5$-12). Data are presented as mean ± SEM; significant differences were determined by the Mann-Whitney test, 2way ANOVA, or one-way ANOVA. *$p < 0.05$, **$p < 0.01$, ***$p < 0.001$, ****$p < 0.0001$

subsequently probed for pSrc, pAKT, pSTAT1, pSTAT3, p-p38, pERK, pJNK, IκBα, GLUT1, HK2, PFK2, cMYC, HIF1α, LDHA, AMPK, Mitofusin-2 and DRP1 (all 1:1000, Cell Signaling Technology), RAPTOR, Notch1 and mTOR (1:1000, Santa Cruz), β-actin (1:3000, Santa Cruz), and anti-rabbit IgG HRP-linked or anti-mouse IgG HRP-linked (1:2500, both Cell Signaling Technology) (Table 3). Detection was performed using the iBright 1500 imaging system (Invitrogen by ThermoFisher Scientific).

Seahorse ATP Rate and Glycolysis Stress Test Kits

Extracellular acidification rate (ECAR) and oxygen consumption rate (OCR) were measured using the Seahorse XF Glycolysis Stress Test kit (Agilent Technologies) according to the manufacturer's instructions. HUVECs (5×10^4 cells/well) were cultured for 2 days before the assay. Syntenin-1 (1 µg/ml) and PBS were injected during the experiment. Glycolysis and glycolytic capacity were calculated by the following equations, respectively: glycolysis = (Maximum rate measurement before Oligomycin injection) – (Last rate measurement before Glucose injection) and glycolytic capacity = (Maximum rate measurement after Oligomycin injection) – (Last rate measurement before Glucose injection). ATP production was calculated by the following equation: ATP production = (Last rate measurement before Oligomycin injection) – (Minimum rate measurement after Oligomycin injection).

Glycolytic ATP production (glycolysis) and mitochondrial ATP production (oxidative phosphorylation) were measured using the Seahorse XF ATP Rate Test kit (Agilent Technologies), according to the manufacturer's instructions. RA FLS (2×10^5 cells/well) were cultured for 1 day and Syntenin-1 (1000 ng/ml) and PBS were injected during the experiment.

Metabolite quantification

Following the manufacturer's instructions, the concentration of the metabolites including Pyruvate, Lactate, Citrate, and Succinate was measured in conditioned media using colorimetric assay kits (Sigma-Aldrich, St. Louis, USA).

Enzyme-Linked-Immunosorbent-Assay (ELISA)

Human TNF-α, IL-1β, CCL5, IL-10, TGFβ, IL-8, and IL-12 protein levels were quantified by ELISA according to the manufacturer's instructions (R&D Systems, Minneapolis, MN).

Immunohistochemistry

RA ST formalin-fixed, paraffin-embedded samples were sectioned and stained for colocalization of Syntenin-1 (1:125), SDC-1 (1:500), VEGFR2 (1:25), Notch1 (1:50), RAPTOR (1:50), HIF1α (1:50), Mitofusin-2 (1:200), and DRP1 (1:200) on VWF^+ endothelial cells (1:1000) and $Vimentin^+$ RA FLS (1:1000). Moreover, fluorescently labeled secondary anti-rabbit (1:200) and anti-mouse (1:200) Abs were utilized to visualize staining. Formalin-fixed mouse ankles were decalcified and paraffin-embedded. Slides were deparaffinized in xylene, and antigen retrieval was achieved as previously described [31]. Mouse ankle sections were stained for Vimentin (1:1000), VWF (1:1000), VEGFR2 (1:25), Notch1 (1:50), MFN2 (1:200), DRP1 (1:200)

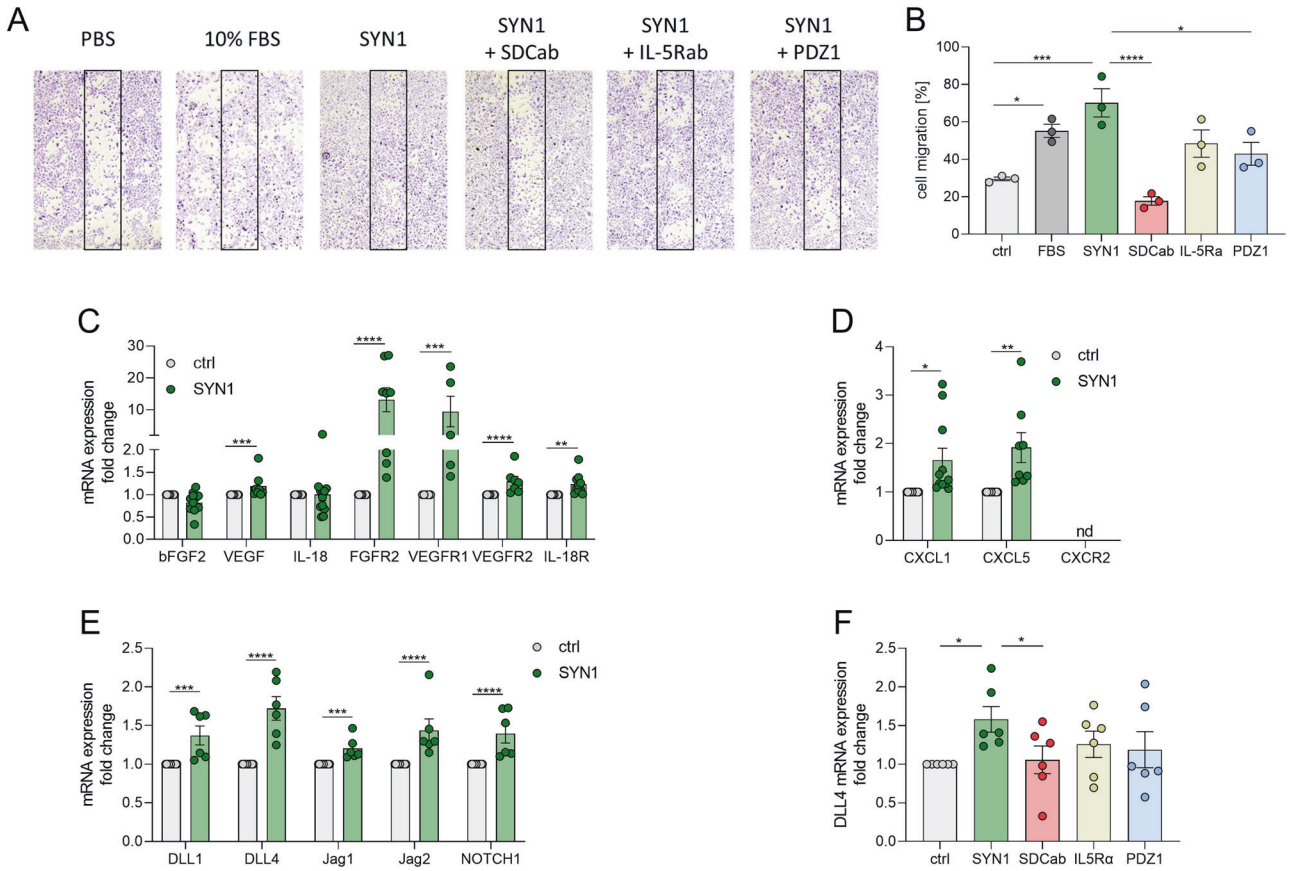

Fig. 2 Syntenin-1 ligation to SDC-1 promotes endothelial cell migration and induction of proangiogenic factors from these cells. **A**. A scratch was created in the middle of the wells that contained confluent HUVECs. Thereafter, cells were either untreated (PBS) or stimulated with Syntenin-1 (1000 ng/ml), or 10% FBS as a positive control for 24h. In parallel, cells were treated with SDC1-Ab (1:100), IL-5R Ab (2 µg/ml), or PDZ1i (10 µM) for 24h, ($n = 3$). **B**. The number of cells in the scratch area was counted and compared to the untreated control, ($n = 3$). **C**–**F**. HUVECs were treated with PBS (ctrl) or Syntenin-1 (1000 ng/ml) in the presence or absence of SDC-1 Ab (SDCab; 1:100), IL-5R Ab (IL5Ra; 2 µg/ml), or PDZ1i (PDZ1; 10 µM) for 6h before quantifying transcription levels of bFGF, VEGF, IL-18, FGFR2, VEGFR1, VEGFR2, IL-18R (**C**), CXCL1, CXCL5, CXCR2 (**D**), DLL1, DLL4, JAG1, JAG2, Notch1 (**E**), and DLL4 (**F**) by qRT-PCR, ($n = 6$-10, nd=not detectable). Data are presented as mean ± SEM; significant differences were determined by the Mann-Whitney test, 2way ANOVA, or one-way ANOVA. *$p < 0.05$, **$p < 0.01$, ***$p < 0.001$, ****$p < 0.0001$

(Tables 4 & 5) and were scored on a scale of 0–5 in a blinded manner (0 = normal appearance, 1 = minimal changes, 2 = mixed appearance, 3 = moderate changes, 4 = marked changes, and 5 = severe changes) [32]. HUVECs were cultured on glass coverslips. Cells were treated with 1000 ng/mL Syntenin-1 for 18h. Cells were fixed with 3.7% paraformaldehyde for 10 min, washed, then permeabilized with 0.1% saponin. Cells were stained with VEGFR2 (1:25) in PBS with 10% NDS and 0.01% sodium azide for 1h at RT. Cells were washed then incubated with DAPI (1:1000) and FITC-fluorescently labeled secondary anti-mouse (1:300) Ab for 20 min. Cells were then washed and mounted on slides for imaging. Mean fluorescence intensity per cell was quantified using NIS-Elements Basic Research software.

Statistical Analysis

For comparison among multiple groups, one-way ANOVA followed by Tukey's multiple comparison tests was employed, using Graph Pad Prism9 software. The data were also analyzed using a two-tailed Student's *t*-test or Mann-Whitney test for paired or unpaired comparisons between two groups. When comparing RNAseq data against continuous or ordinal variables, the Spearman rank correlation test was used, and Spearman rho and p-values are shown. $p < 0.05$ was considered statistically significant.

RESULTS

Syntenin-1 and SDC-1 are co-expressed on RA ST endothelial cells and Syntenin-1 amplifies inflammatory reconfiguration in endothelial cells

RNAseq data revealed that the expression of Syntenin-1 and SDC-1 in RA ST and blood were comparable in RA patients who were nonresponsive compared to those with moderate (DAS28 change ≤1.2 and >0.6) and good response (DAS28 change >1.2) (Fig. 1A, B & Suppl. 1A-B). Corroborating these findings, RA synovial Syntenin-1 and SDC-1 transcriptomes were unchanged in RA patients that displayed good response to anti-TNF (Certolizumab, Suppl. 1C-D), and anti-IL-6R Ab (Tocilizumab, Suppl. 1E-F) relative to non-responders. Intriguingly, Syntenin-1 and SDC-1 were co-localized on RA ST endothelial cells, suggesting that cells producing Syntenin-1 were also responsive to its stimulation (Fig. 1C). HUVECs activated by Syntenin-1 exhibited ERK and p38 MAPK signaling together with transient IκB degradation, while JNK, AKT, STAT1/3 cascades were unaffected (Fig. 1D).

Moreover, expression of a wide range of transcription factors (IRF1/3/4/5/7/8/9) along with inflammatory mediators including

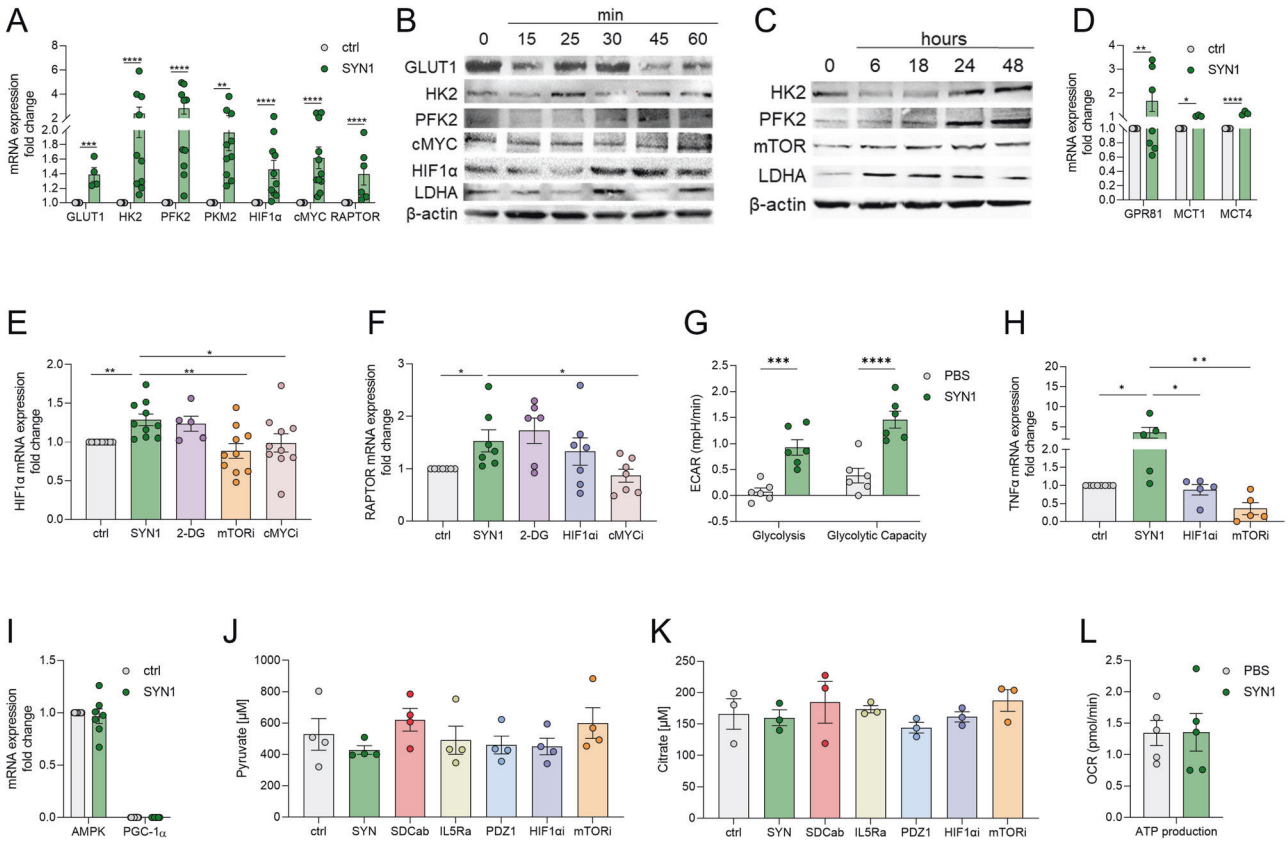

Fig. 3 Syntenin-1 reprogrammed endothelial cells display accelerated glycolytic activity with no effect on oxidative phosphorylation. **A**. HUVECs were treated with PBS (ctrl) or Syntenin-1 (1000 ng/ml) for 6h and transcription of the glycolytic factors GLUT1, HK2, PFK2, PKM2, HIF1α, cMYC, RAPTOR (**A**) was determined by qRT-PCR. **B, C**. HUVECs were treated with Syntenin-1 (1000 ng/ml) for 0-60 minutes to detect expression of GLUT1, HK2, PFK2, cMYC, HIF1α, and LDHA (**B**) or 0-48h to detect HK2, PFK2, mTOR/RAPTOR and LDHA (**C**), β-actin served as a loading control, ($n = 3$). **D-F** HUVECs were treated with PBS or Syntenin-1 (1000 ng/ml) in the presence or absence of 2-DG (5 mM), mTORi (1 μM), HIF1αi (2 μM) or cMYCi (50 μM) to quantify transcription of Lactate receptor (GPR81) and transporters (MCT1/4) (**D**), HIF1α (**E**), and RAPTOR (**F**). **G**. Using a Seahorse XF Glycolysis Stress Test Kit from Agilent (cat# 103020-100), ECAR was evaluated in HUVECs treated with PBS and Syntenin-1 (1000 ng/ml) for 0-112 min and data are shown as Glycolysis and Glycolytic Capacity, ($n = 6$). **H, I**. Transcription of TNFα (**H**) and AMPK and PGC-1α (**I**) in HUVECs was established by qRT-PCR after 6h of treatment with Syntenin-1 (1000 ng/ml) in the presence or absence of HIF1αi (2 μM) and mTORi (1 μM) ($n = 5$-7). **J, K**. HUVECs were treated with PBS or Syntenin-1 (1000 ng/ml) in the presence or absence of SDC-1 Ab (SDCab; 1:100), IL-5R Ab (IL5Ra; 2 μg/ml), PDZ1i (PDZ1; 10 μM), HIF1αi (2 μM) or mTORi (1 μM) for 24h before measuring Pyruvate (**J**) or Citrate (**K**) levels by a colorimetric assay, ($n = 3$-4). **L**. Employing a Seahorse XF Glycolysis Stress Test Kit from Agilent (cat# 103020-100), OCR was evaluated in HUVECs treated with PBS and Syntenin-1 (1000 ng/ml) for 0-112 min and data were shown as ATP production, ($n = 5$). Data are presented as mean ± SEM; significant differences were determined by the Mann-Whitney test, 2way ANOVA, or one-way ANOVA. *$p < 0.05$, **$p < 0.01$, ***$p < 0.001$, ****$p < 0.0001$

IL-1β, IL-6, TNF, IL-8, CCL2, and CCL5 were upregulated at the transcriptional and translational levels in HUVECs reprogrammed by Syntenin-1 (Fig. 1E, F, G–I). Notably, while SDC-1 Ab constrained Syntenin-1-induced IL-1β and TNF transcription, blockade of IL-5R or PDZ1 did not influence this process (Fig. 1J, K). Syntenin-1 activation also augmented HUVEC responsiveness to TLR ligands by advancing both the cell surface (TLR2/4/5) and the endosomal TLRs (TLR7) (Fig. 1L). In contrast, the pro-repair phenotype, IL-10, and TGFβ were uninvolved in HUVECs remodeled by Syntenin-1 (Fig. 1M). In short, endothelial cells exposed to Syntenin-1 display a strong inflammatory profile that is primarily dependent on SDC-1 ligation.

Syntenin-1 is responsible for endothelial cell migration and expression of pro-angiogenic factors

Given that Syntenin-1 and SDC-1 are colocalized on RA vasculature, we examined other manifestations of this pathway on HUVECs as RA endothelial cell substitutes. We found that endothelial cells migrate in response to Syntenin-1 via SDC-1 or PDZ1, which was unaffected by anti-IL-5R antibody (Ab) (Fig. 2A, B). Further, transcription of numerous proangiogenic factors was markedly expanded in HUVECs reconfigured by Syntenin-1 which included VEGF, CXCL1, CXCL5, DLL1, DLL4, JAG1, and JAG2 (Fig. 2C–E). Consistently, levels of FGFR2, VEGFR1/2, IL-18R, and Notch1 were also amplified in HUVECs through Syntenin-1 exposure (Fig. 2C–E).

Data generated in RA ST explants, and/or FLS highlighted the significance of VEGF and VEGFR1/2 and JAG1/Notch1 in Syntenin-1-induced pathology (Figs. 9G, I, and 6L, M). In agreement, VEGFR1/2 and Notch1, as well as their complementary ligands, were highly expressed in endothelial cells in response to Syntenin-1 (Fig. 2C, E, Suppl. 1K-M). However, in some instances, either the ligand (bFGF2, IL-18) or the receptor (CXCR2) remained undetected (Fig. 2C, D). Similar to endothelial cell-enhanced inflammation and infiltration, SDC-1 was responsible for Synteinin-1-mediated DLL4 transcription (Fig. 2F). Taken together, angiogenesis is advanced both directly and indirectly by ligation of Syntenin-1 to SDC-1^{+}endothelial cells in part through VEGFR and Notch1 networks.

HIF1α and RAPTOR activation promote Syntenin-1 metabolic reprogramming in endothelial cells

Next, experiments were conducted to determine whether the endothelial inflammatory landscape is influenced by metabolic rewiring by Syntenin-1. Syntenin-1 reprogramming of endothelial cells resulted in transcriptional upregulation of a wide range of glycolytic intermediates, GLUT1, HK2, PFK2, PKM2, HIF1α, cMYC, and RAPTOR (Fig. 3A). Contrary to transcriptional upregulation of GLUT1, its translation levels were unaffected

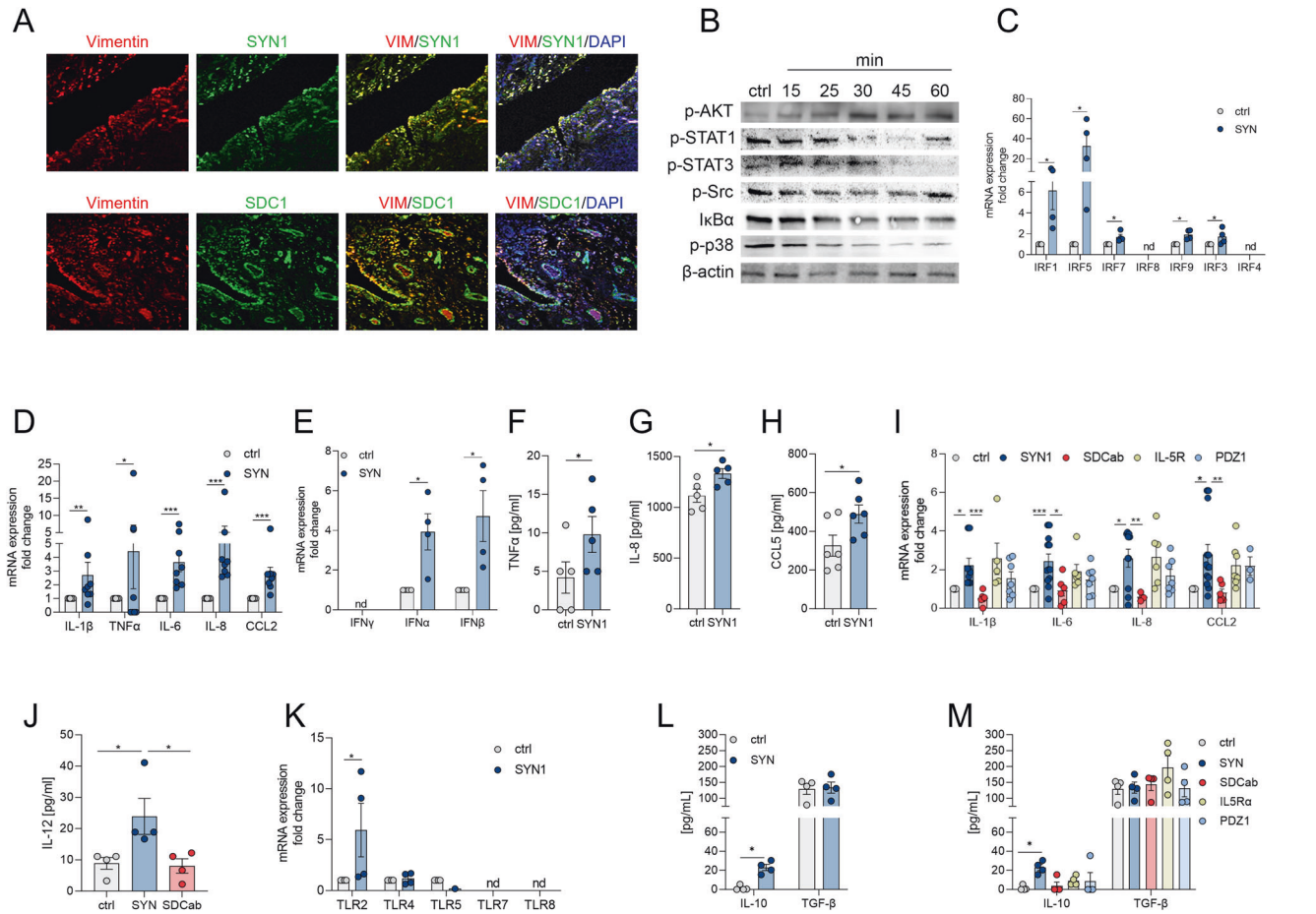

Fig. 4 The inflammatory profile surpasses the pro-repair phenotype in Syntenin-1 reprogrammed RA FLS. **A**. RA STs were fluorescently stained to authenticate the colocalization of SDC-1 and Syntenin-1 expression on Vimentin^{+}FLS in the presence or absence of DAPI, ($n = 3$, original magnification x 20). **B**. RA FLS were treated with Syntenin-1 (1000 ng/ml) for 0-60 mins and phosphorylation of AKT, STAT1, STAT3, Src, p38, or degradation of IκBα was determined by western blot analysis and β-actin served as a loading control, ($n = 3$). **C–M**. RA FLS were treated with PBS (ctrl) or Syntenin-1 (1000 ng/ml) in the presence or absence of SDC-1 Ab (SDCab; 1:100), IL-5R Ab (IL5Ra; 2 μg/ml), or PDZ1i (PDZ1; 10 μM) for 6h or 24h before quantifying transcriptional or translational levels of IRFs (**C**, $n = 4$), inflammatory mediators (**D–I**, $n = 4$-9), IL-12 (**J**, $n = 4$), TLRs (**K**, $n = 4$) and pro-repair factors (**L, M**, $n = 4$) by qRT-PCR or ELISA. Data are presented as mean ± SEM; significant differences were determined by the Mann-Whitney test, 2way ANOVA, or one-way ANOVA. *$p < 0.05$, **$p < 0.01$, ***$p < 0.001$, ****$p < 0.0001$

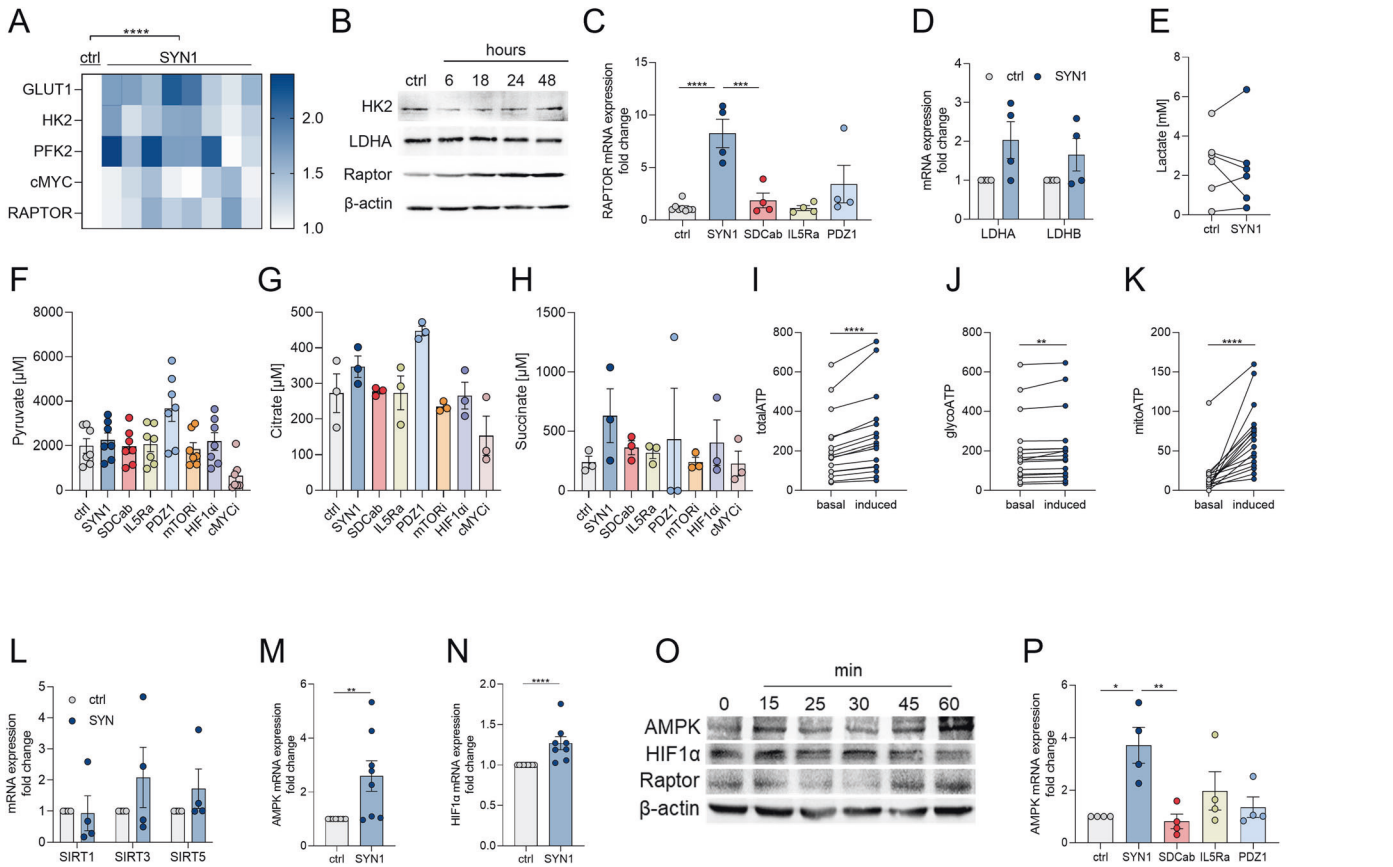

Fig. 5 RA FLS reprogrammed by Syntenin-1 display dysregulated mitochondrial oxidative stress. RA FLS were treated with PBS (ctrl) or Syntenin-1 (1000 ng/ml) for 6h and transcription of glycolytic mediators GLUT1, HK2, PFK2, cMYC, and RAPTOR was determined by qRT-PCR (**A**, $n = 8$). RA FLS were treated with Syntenin-1 (1000 ng/ml) for 0-48h to detect HK2, LDHA, and RAPTOR (**B**, $n = 3$). **C–H**. RA FLS were treated with PBS (ctrl) or Syntenin-1 (1000 ng/ml) in the presence or absence of SDC-1 Ab (SDCab; 1:100), IL-5R Ab (IL5Ra; 2 μg/ml), PDZ1i (PDZ1; 10 μM), mTORi (1 μM), HIF1αi (2 μM) or cMYCi (50 μM) for 6h (mRNA) or 24h (protein) and transcription of glycolytic mediators, RAPTOR (**C**, $n = 4$), LDHA, LDHB (**D**, $n = 4$) and protein expression of Lactate (**E**), Pyruvate (**F**), Citrate (**G**), and Succinate (**H**) ($n = 3$-7) were determined by qRT-PCR, or colorimetric assay. **I–K**. RA FLS were treated with PBS (basal) or Syntenin-1 (1000 ng/ml, induced), and total ATP (**I**), glycoATP (**J**), and mitoATP (**K**) were determined by Seahorse XF Real-Time ATP Rate Assay Kit ($n = 13$). **L–N**. RA FLS were treated with PBS or Syntenin-1 (1000 ng/ml) for 6h before quantifying transcription of metabolic intermediates; SIRT1, SIRT3, SIRT5 (**L**, $n = 4$) or AMPK (**M**, $n = 8$) and HIF1α (**N**, $n = 8$) by qRT-PCR. RA FLS were treated with Syntenin-1 (1000 ng/ml) for 0-60 minutes to detect AMPK, HIF1α, or RAPTOR protein levels (**O**, $n = 3$). **P**. RA FLS were treated with PBS or Syntenin-1 (1000 ng/ml) in the presence or absence of SDC-1 Ab (SDCab; 1:100), IL-5R Ab (IL5Ra; 2 μg/ml), or PDZ1i (PDZ1; 10 μM) for 6h before quantifying transcription levels of AMPK ($n = 4$). In western blot analysis, β-actin served as a loading control. Data are presented as mean ± SEM; significant differences were determined by the Mann-Whitney test, 2way ANOVA, or one-way ANOVA. *$p < 0.05$, **$p < 0.01$, ***$p < 0.001$, ****$p < 0.0001$

by Syntenin-1 in HUVECs (Fig. 3B, Suppl. 1H). While HK2, PFK2, and LDHA protein levels were transiently enhanced at short-term Syntenin-1 activation, their levels were more stably elevated in HUVECs following 24h and 48h of stimulation (Fig. 3B, C, Suppl. 1G). Moreover, HIF1α, cMYC, and mTOR/RAPTOR protein levels were enriched in Syntenin-1 reprogrammed HUVECs (Fig. 3B, C).

Interestingly, lactate specific receptor on endothelial cells, GPR81, as well as its transporters MCT1 (importer) and MCT4 (exporter) were potentiated by Syntenin-1 (Fig. 3D). The data suggest that following Syntenin-1 stimulation, there is dynamic glycolysis that occurs by lactate being sensed through amplified endothelial GPR81 frequency as well as the activity of the transporters directing its import or export.

Additionally, Syntenin-1-elevated HIF1α and RAPTOR expression levels are suppressed by cMYCi, whereas HIF1α can also be dysregulated by mTORi (Fig. 3E, F). In endothelial cells reprogrammed by Syntenin-1, HIF1α, and RAPTOR signaling are linked to the amplification of glycolysis and glycolytic capacity as well as the inflammatory phenotype (Fig. 3G, H). Corroborating with this notion, TNF expression was diminished by HIF1αi and mTORi in Syntenin-1-reconfigured endothelial cells, yet cMYCi did not replicate this function (Fig. 3H).

The oxidative metabolites, AMPK, PGC-1α, and Citrate were unaltered in endothelial cells reprogrammed by Syntenin-1 and consequentially unchanged by HIF1αi and mTORi therapy (Fig. 3I–K). cMYCi treatment was uniquely capable of advancing Pyruvate and Citrate levels in Syntenin-1 reprogrammed endothelial cells (Suppl. 1I-J). Distinct from the robust induction of glycolysis and its intermediates delineated in endothelial cells reconfigured by Syntenin-1, OCR and oxidative metabolites were uninvolved in these cells (Fig. 3I–L). Altogether endothelial cells are metabolically reprogrammed by Syntenin-1 in part through HIF1α and mTOR activation.

RA FLS remodeled by Syntenin-1 display inflammatory imprint

Morphological studies elucidated that both Syntenin-1 and SDC-1 are co-localized on Vimentin$^+$ RA FLS (Fig. 4A). Syntenin-1 stimulated RA FLS signal through AKT and NF-κB with no effect on STAT1/3, Src, or p38 activation (Fig. 4B). Reprogramming of RA FLS by Syntenin-1 coincides with expanded IRF1/5/7/9/3 along

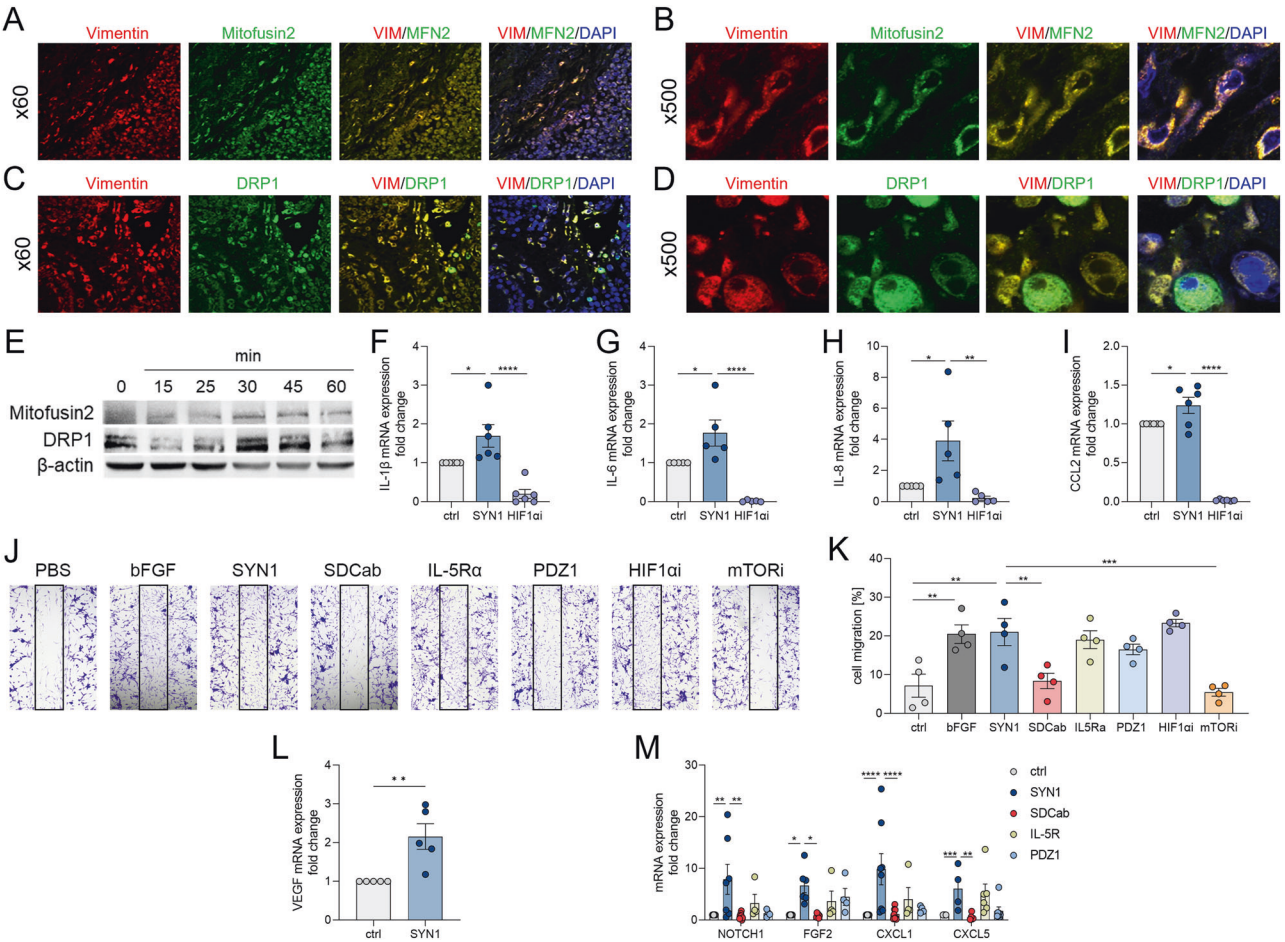

Fig. 6 Syntenin-1 rewired RA FLS exhibit mitochondrial fusion and fission, in addition, the inflammatory phenotype was differentially regulated compared to RA FLS migration in response to Syntenin-1. **A–D**. RA STs were fluorescently stained to authenticate the colocalization of Mitofusin-2 (MFN2) (**A, B**) and DRP1 (**C, D**) expression on Vimentin$^+$ FLS in the presence or absence of DAPI, ($n = 3$, original magnification x 60 or x500). **E**. RA FLS were treated with Syntenin-1 (1000 ng/ml) for 0-60 min to detect Mitofusin-2 and DRP1 expression by western blot, β-actin served as a loading control, ($n = 3$). **F–I**. RA FLS were treated with Syntenin-1 (1000 ng/ml) in the presence or absence of HIF1αi (2 μM) for 6h to determine transcription of IL-1β (**F**, $n = 6$), IL-6 (**G**, $n = 5$), IL-8 (**H**, $n = 5$) and CCL2 (**I**, $n = 6$) by qRT-PCR. **J, K**. A scratch was created in the middle of the wells that contained confluent RA FLS. Thereafter, cells were either untreated (PBS) or stimulated with Syntenin-1 (1000 ng/ml), or bFGF (100 ng/ml) as a positive control for 24h. In parallel, cells were treated with SDC-1 Ab (SDCab, 1:100), IL-5R Ab (IL5Ra, 2 μg/ml), PDZ1i (PDZ1, 10 μM), HIF1αi (2 μM) or mTOR1i (1μM) for 24h, (**J**, $n = 4$). The number of cells in the scratch area was counted and compared to the untreated control, (**K**, $n = 4$). **L, M**. RA FLS were treated with PBS or Syntenin-1 (1000 ng/ml) in the presence or absence of SDC-1 Ab (SDCab; 1:100), IL-5R Ab (IL5Ra; 2 μg/ml), or PDZ1i (PDZ1; 10 μM) for 6h before quantifying transcription levels of VEGF (**L**, $n = 5$) or Notch1, FGF2, CXCL1, and CXCL5 (**M**, $n = 6$-8). Data are presented as mean ± SEM; significant differences were determined by the Mann-Whitney test, 2way ANOVA, or one-way ANOVA. *$p < 0.05$, **$p < 0.01$, ***$p < 0.001$, ****$p < 0.0001$

with a robust inflammatory phenotype that reveals induction of IL-1β, IL-6, TNF, IL-8, CCL2, CCL5, IFNα, and IFNβ transcriptome and/or protein levels (Fig. 4C–H). The inflammatory remodeling of RA FLS by Syntenin-1 and enhancement of IL-1β, IL-6, IL-8, CCL2, and IL-12 were impaired by SDC-1 Ab but not PDZ1i (Fig. 4I, J).

However, unlike endothelial cells, TLR amplification in RA FLS exposed to Syntenin-1 was restricted to TLR2 (Fig. 4K). Also distinct from HUVECs, RA FLS remodeled by Syntenin-1 displayed higher IL-10 expression, unlike TGFβ which was unaffected in both cell types (Fig. 4L, M). Collectively, our results suggest that RA FLS reprogramming by Syntenin-1 is accompanied by a predominant inflammatory phenotype that exceeds the pro-repair profile.

RA FLS remodeled by Syntenin-1 have a unique metabolic profile

Next, the metabolic functionality of RA FLS remodeling by Syntenin-1 was analyzed to characterize its participation in different implications. In RA FLS, Syntenin-1 stimulation was capable of promoting a modest transcriptional induction of GLUT1, HK2, PFK2, cMYC, and RAPTOR but not PKM2 (Fig. 5A, Suppl. 2A-F). Furthermore, elevated RAPTOR protein expression was captured in RA FLS reprogrammed by Syntenin-1 following short (45-60 min) and long exposure (18h-48h) (Fig. 5B, O). RAPTOR expression levels were counteracted by SDC-1 Ab but not IL-5R Ab or PDZ1i in RA FLS rewired by Syntenin-1 (Fig. 5C). In parallel, neither lactate catalyzing enzymes (LDHA or LDHB) nor accumulation of Pyruvate or Lactate were impacted in Syntenin-1-remodeled RA FLS (Fig. 5D–F).

Concurrently, secretion of oxidative metabolites including Citrate and Succinate was unaffected in Syntenin-1-rewired RA FLS (Fig. 5G, H). Nonetheless, RA FLS exposed to Syntenin-1 showed a marked increase in total ATP levels which was accompanied by a modest glycoATP and a more intense mitoATP activity (Fig. 5I–K). In evaluating other oxidative intermediates in Syntenin-1-reprogrammed RA FLS, while SIRT1/3/5 were unaffected (Fig. 5L), transcription and translation levels of AMPK and HIF1α were

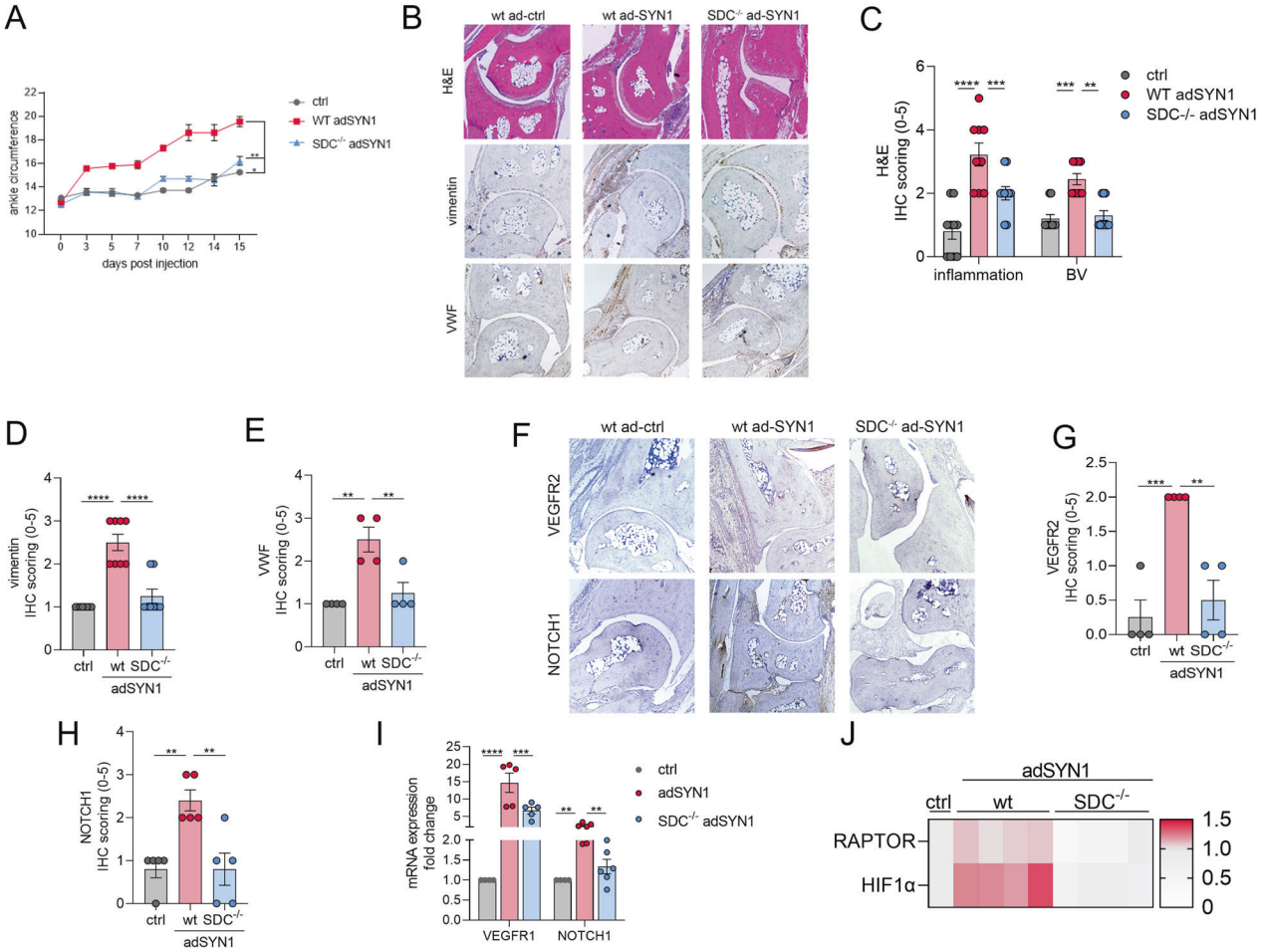

Fig. 7 Syntenin-1 arthritic mice recapitulate RA pathology by exhibiting Vimentin^{+} fibroblast and VWF^{+} endothelial cell recruitment in WT mice which was mitigated in SDC-1$^{-/-}$ animals. **A**. WT and SDC-1$^{-/-}$ mice were injected intra-articularly with ad-ctrl (ctrl) or adSYN1 (3×10^{10} viral particles/ankle) on days 0, 7, and 14 and joint circumference was monitored over 15 days ($n = 10$ mice/group). Ankles from non-arthritic WT ctrl and WT or SDC-1$^{-/-}$ mice injected with ad-SYN1 were stained for H&E, Vimentin, and VWF (**B**) or VEGFR2 and Notch1 (**F**), and their staining was scored on a 0-5 scale (**C, D, E, G, H**; $n = 4$-9). The ankles from non-arthritic WT ctrl and WT or SDC$^{-/-}$ mice injected with ad-SYN1 were homogenized and transcriptional regulation of VEGFR1 and Notch1 (**I**) or RAPTOR, and HIF1α (**J**) was determined by qRT-PCR ($n = 4$-6). Data are presented as mean ± SEM; significant differences were determined by the Mann-Whitney test, 2way ANOVA, or one-way ANOVA. *$p < 0.05$, **$p < 0.01$, ***$p < 0.001$, ****$p < 0.0001$

significantly potentiated (Fig. 5M–O) and further manipulated by SDC-1 ligation (Fig. 5P). Despite the lack of Succinate accumulation in Syntenin-1-remodeled RA FLS (Fig. 5H), mitochondrial oxidative phosphorylation is shown to be related to AMPK and HIF1α activation [33–35]. We also elucidated that the stark mitoATP activity observed in Syntenin-1-reprogrammed RA FLS (Fig. 5K) was coupled with mitochondrial fusion and fission signified by escalated Mitofusin-2 and DRP1 (Fig. 6A–E). We showed that Mitofusin-2 and DRP1 are colocalized on Vimentin^{+} RA FLS and Syntenin-1 exposure enhances their protein expression (Fig. 6A–E, Suppl. 2G-H). Remarkably, HIF1αi strongly impaired the inflammatory reconfiguration of RA FLS by Syntenin-1 and led to the downregulation of IL-1β, IL-6, IL-8, and CCL2 transcription (Fig. 6F–I). Meanwhile, Syntenin-1-driven RA FLS migration was intercepted by SDC-1 Ab and mTORi but not HIF1αi (Fig. 6J, K). Extending our findings with HUVECs, RA FLS exposed to Syntenin-1 revealed transcriptional enrichment of pro-angiogenic mediators including VEGF and/or Notch1, FGF2, CXCL1, and CXCL5 which were singularly constrained by SDC-1 Ab (Fig. 6L, M). Taken together, while metabolic dysregulation via HIF1α manipulates Syntenin-1 expanded inflammatory network in RA FLS, mTOR signaling is involved in RA FLS migration in response to Syntenin-1.

Syntenin-1-induced pathology is mitigated by SDC-1 disruption and RAPTOR or HIF1α deactivation

Local injection of adenovirus (ad)-Syntenin-1 resulted in progressive arthritic joint inflammation in wild-type mice compared to SDC-1 KO mice that received ad-Syntenin-1 or ad-ctrl administration (Fig. 7A). Ectopic expression of Syntenin-1 in WT mice was manifested by escalated joint inflammation and blood vessel formation (BV) accompanied by the expansion of Vimentin^{+} fibroblasts and VWF^{+} endothelial cells which were obstructed in SDC-1$^{-/-}$ animals (Fig. 7B–E). Morphological and transcriptome studies recapitulate the importance of VEGFR1/2, Notch1, RAPTOR, and HIF1α pathways in Syntenin-1-induced arthritis and their dysregulation in SDC-1$^{-/-}$ mice compared to the control animals (Fig. 7F–J). In line with these findings, expression of GLUT1 and HK2 was upregulated in joint Vimentin^{+} fibroblasts and VWF^{+} endothelial cells in the wild-type ad-Syntenin-1 arthritic mice compared to ctrl or SDC1$^{-/-}$ ad-Syntenin-1 groups (Suppl. 3 and Suppl. 4).

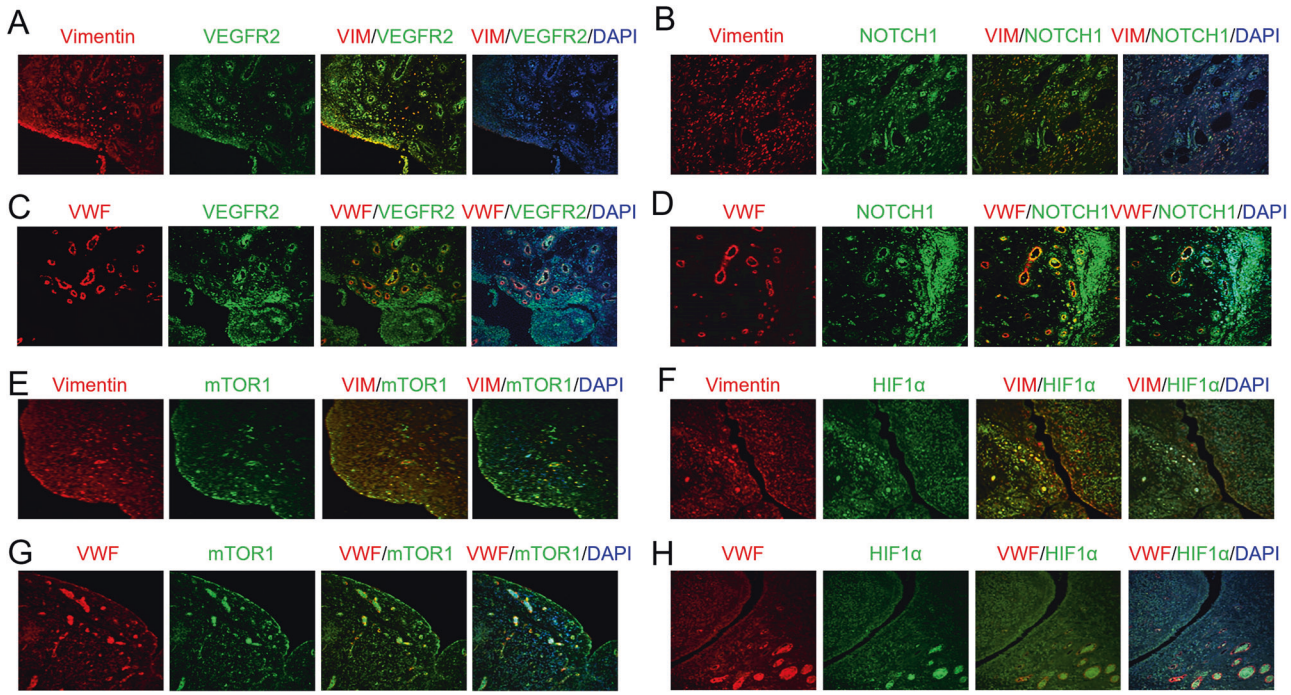

Fig. 8 VEGFR2, Notch1, RAPTOR, and HIF1α are represented in RA ST FLS and endothelial cells. RA STs were fluorescently stained to authenticate the colocalization of VEGFR2 (**A, C**), Notch1 (**B, D**), mTOR1 (**E, G**), and HIF1α (**F, H**) on Vimentin$^+$ FLS and VWF$^+$ endothelial cells in the presence or absence of DAPI, ($n = 3$, original magnification x 20)

Intriguingly, in Syntenin-1-induced arthritis, we illustrate that VEGFR2 (Fig. 8A, C), Notch1 (Fig. 8B, D), mTOR (Fig. 8E, G), and HIF1α (Fig. 8F, H) are co-expressed on Vimentin$^+$ RA FLS and VWF$^+$ RA endothelial cells by IF staining. Authenticating the morphological findings, single-cell RNAseq displays that Syntenin-1 and HIF1α are widely expressed on RA FLS and ST endothelial cells, while SDC-1 and RAPTOR are modestly presented on these cell types (Fig. 9A-D). At the onset of these studies, our goal was to define the interplay between endothelial cells and RA FLS in response to Syntenin-1 in coculture. However, because HUVECs require a high growth factor milieu for optimal proliferation, the coculture is taken over by RA FLS leading to endothelial cell death. Hence these experiments were performed in explants where RA FLS are in direct contact with the endothelium (Fig. 9E).

To evaluate the functional significance and cross-regulation of VEGFR, Notch1, and inflammatory phenotype in connection with SDC-1 ligation or RAPTOR and HIF1α activation, RA explants were exposed to Syntenin-1 in the presence or absence of SDC-1 Ab, mTORi or HIF1αi. JAG1, Notch1, VEGF, VEGFR1, and RAPTOR transcription levels were amplified in RA ST explants stimulated by Syntenin-1 (Fig. 9F–J). We noted that Syntenin-1-enriched RAPTOR expression was suppressed both by mTOR and HIF1α inhibitors (Fig. 9K). In light of these findings, HIF1αi was capable of negating the expression of VEGF (Fig. 9L) and numerous inflammatory mediators such as IL-6, IL-8, and TNF in RA explants in response to Syntenin-1 (Fig. 9O, P, R). While SDC-1 Ab was responsible for restricting IL-1β and CCL5 transcription (Fig. 9M, N), mTORi intercepted CCL2 transcription and TNF secretion in RA explants exposed to Syntenin-1 (Fig. 9Q, R). Collectively, our data suggest that Syntenin-1-escalated inflammatory and/or proangiogenic landscapes in endothelial cells, RA FLS, and RA explants are primarily modulated by SDC-1 and HIF1α. Whereas mTOR activity has a more restricted influence on Syntenin-1-expanded inflammatory profile in endothelial cells and RA explants as well as migration of RA FLS.

DISCUSSION

This study unmasks the pathology of a novel RA synovial fluid protein, Syntenin-1, that can reprogram endothelial cells and RA FLS by molding their inflammatory and angiogenic landscapes with metabolic activity. Our findings show that Syntenin-1 remodels the inflammatory imprint of endothelial cells and RA FLS by activating IRF1/5/7/9 alongside expanding the transcription of IL-1β, IL-6, and CCL2 via SDC-1 ligation, HIF1α, and/or mTOR activation. Nevertheless, the Syntenin-1-driven metabolic reconfiguration is quite distinct in endothelial cells relative to RA FLS. Syntenin-1 rewired endothelial cells display elevated glycolytic capacity with robust activation of RAPTOR and HIF1α, while the mitochondrial oxidative phosphorylation is unaffected as corroborated by unchanged OCR and AMPK levels. Uniquely, RA FLS reprogrammed by Syntenin-1 showed a modest glycoATP together with a more prominent mitoATP activity. This RA FLS phenotype is signified by elevated oxidative stress and altered mitochondrial dynamics facilitated through amplified AMPK, HIF1α, and Mitofusin-2, or DRP1. Our findings in endothelial cells and RA FLS are recapitulated in murine arthritic joints and RA explants, where Syntenin-1 plays a critical role in guiding the inflammatory and angiogenic networks through VEGFR and Notch1 via HIF1α and RAPTOR involvement. In short, Syntenin-1 may be a novel inducer of RA pannus through its ability to link the inflammatory, angiogenic, and metabolic networks of endothelial cells with RA FLS (Fig. 10).

Syntenin-1 and SDC-1 were discovered by RNAseq studies, where their expression in RA STs was linked to CD68$^+$ sublining cells, ESR, and/or ultrasound ST thickness [14, 16]. The Syntenin-1/SDC-1 pathway became a more attractive therapeutic target when its expression was found to be unaffected in responders who were treated with DMARDs or biologics. These findings led us to investigate whether Syntenin-1 and SDC-1 expression expanded beyond RA myeloid cells. Intriguingly, Syntenin-1 and SDC-1 are colocalized on RA ST VWF$^+$ endothelial cells and Vimentin$^+$ RA FLS as revealed by single-cell RNAseq analysis [26].

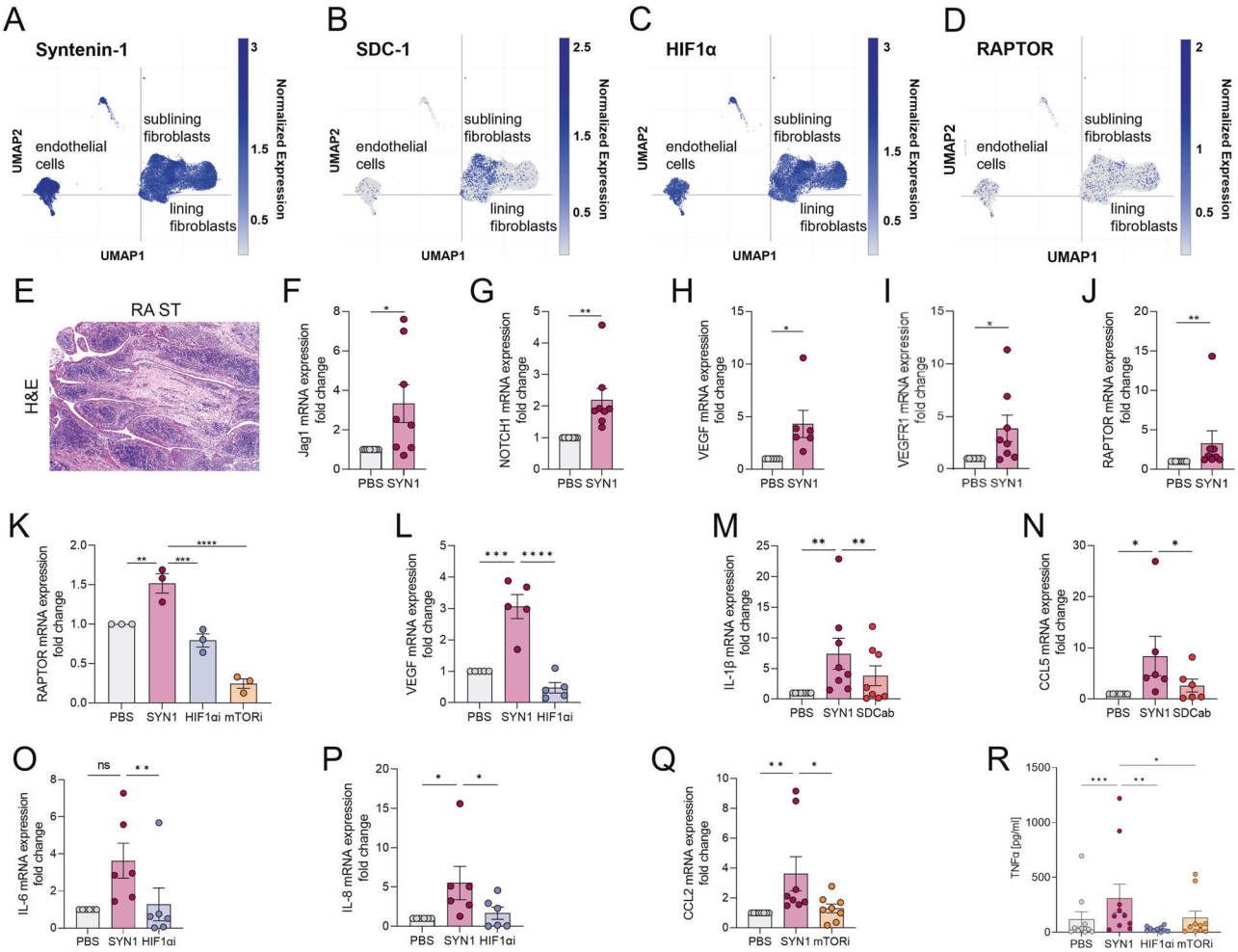

Fig. 9 Syntenin1-induced metabolic activity fine-tunes transcription of angiogenic and inflammatory factors in RA ST explants. Normalized expression levels of Syntenin-1 (**A**), SDC-1 (**B**), HIF1α (**C**), and RAPTOR (**D**) are displayed on the lining and sublining RA FLS as well as endothelial cells based on single-cell RNA sequencing data from Wei et al. [26]. **E**. A representative RA ST utilized in Fig. F-R is shown. **F–R**. RA STs (30 mg) were cut into small pieces to allow proper access to stimuli and were starved o/n in 0% FBS RPMI with or without SDC-1-Ab (1:100), mTOR1i (1 μM), and HIF1αi (2 μM). RA STs were stimulated with 1000 ng/ml Syntenin-1 for 6-8h. Synovial tissues were harvested for transcriptome analysis by qRT-PCR and supernatants were used for protein quantification by ELISA. The transcription levels of JAG1 (**F**), Notch1 (**G**), VEGF (**H, L**), VEGFR1 (**I**), and RAPTOR (**J, K**) as well as IL-1β (**M**), CCL5 (**N**), IL-6 (**O**), IL-8 (**P**), and CCL2 (**Q**) were quantified by qRT-PCR, $n = 3$-8. **R**. Production of TNFα was evaluated by ELISA, ($n = 10$). Data are presented as mean ± SEM; significant differences were determined by the Mann-Whitney test, 2way ANOVA, or one-way ANOVA. *$p < 0.05$, **$p < 0.01$, ***$p < 0.001$, ****$p < 0.0001$

We found that endothelial cells reprogrammed by Syntenin-1 displayed a robust inflammatory phenotype that was exhibited by activation of ERK, p38, and NF-κB as well as transcriptional upregulation of IRFs, IL-1, IL-6, IL-8, TNF, CCL2, CCL5, and numerous TLRs. In contrast, the pro-repair phenotype, through IL-10 and TGFβ, was uninvolved in endothelial cells exposed to Syntenin-1. Syntenin-1 ligation to SDC-1 directly advanced endothelial cell migration. Concurrently, upregulation of the proangiogenic factors (VEGF, DLL1/4 and JAG1/2) and their complementary receptors, VEGFR and Notch1, supported the indirect role of Syntenin-1 on angiogenesis. Earlier studies have reported that Syntenin-1 interaction with VEGFR and ephrin-B2 in endothelial cells expands VEGF-mediated angiogenesis [36]. Others have shown that the production of Insulin Growth Factor Binding Protein-2 (IGFBP-2) from melanoma cells activated by Syntenin-1 is responsible for VEGF secreted from HUVECs [37]. Previous reports also demonstrate that overexpression of SDC-1 in mesothelioma cells dysregulates endothelial cell migration and tube formation [38]. Distinctly, we exhibit the importance of SDC-1 ligation for endothelial cell migration and angiogenic factor expression in response to Syntenin-1.

Extensive similarities were noted between RA MΦs and endothelial cells reprogrammed by Syntenin-1, as both cell types demonstrated escalated ECAR activity that was accompanied by elevated GLUT1, HK2, PFK2, HIF1α, and RAPTOR [14]. While OCR and AMPK levels were unaffected in endothelial cells reprogrammed by Syntenin-1, mitoATP and AMPK transcription were reduced in Syntenin-1-differentiated MΦs [14]. In Syntenin-1 reconfigured endothelial cells the inflammatory imprint was reversed by HIF1αi and mTORi treatment. Whereas, the inflammatory and metabolic ($CD14^+CD86^+GLUT1^+$) networks expanded in RA MΦs rewired by Syntenin-1 were exclusively impaired by mTORi primarily due to glucose uptake [14]. We found that endothelial cells reprogrammed by TNF were distinct from those rewired by Syntenin-1, as exposure to TNF resulted in a distinct profile that was exhibited by upregulated GLUT4, PFK2, and downregulated PDK4 along with enhanced ECAR and OCR [39]. These authors delineated that the inflammatory and metabolic activity observed in TNF reconfigured endothelial cells was disrupted by blocking NF-κB and PFK2 function [39]. Furthermore, mitochondrial pyruvate carrier inhibition enhanced PDK4 transcription and the inflammatory phenotype

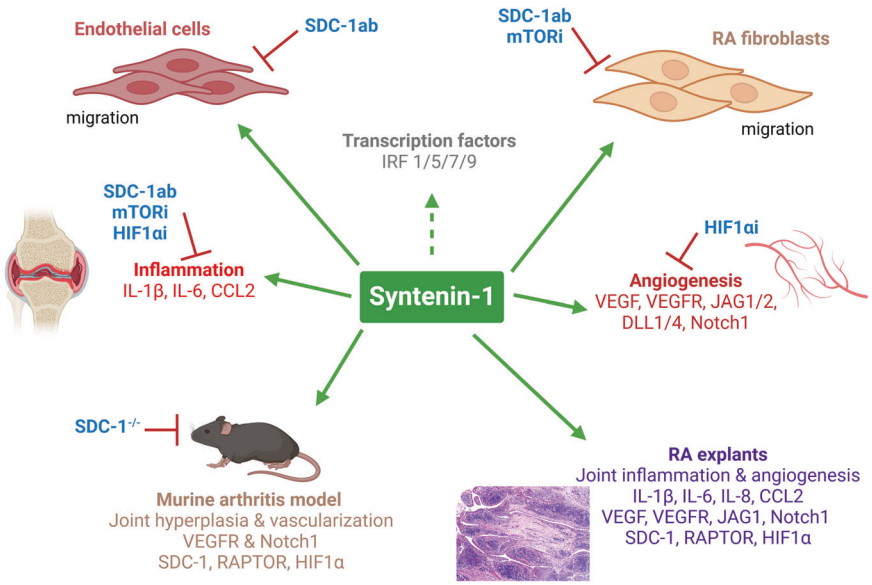

Fig. 10 The Syntenin-1/SDC-1 pathway influences RA FLS and endothelial cell pathology in RA explants and experimental models. The schematic figure demonstrates the mechanism by which Syntenin-1 reprograms endothelial cells and RA FLS and how inflammatory and angiogenic markers are impacted by SDC-1 and metabolic intermediates

along with restraining OCR advanced by TNF-remodeled endothelial cells [39]. Contrasting this observation, OCR was unchanged and disconnected from the inflammatory landscape detected in Syntenin-1 reprogrammed endothelial cells. Others have shown glycolysis activation via PFK2 is responsible for VEGF-induced angiogenesis [40], yet our observation suggests that HIF1α-induced signaling is responsible for VEGF expression and function in RA STs.

RA FLS remodeled by Syntenin-1 and those differentiated by LPS/IFNγ were capable of activating AKT and NF-κB signaling as well as upregulating IRF1/5/7 along with IL-6, IL-8, and CCL2, which was reversed by SDC-1 Ab or 2-DG and IACS (Complex1i) respectively [41]. Syntenin-1 reprogramming did not impact IL-10 and TGFβ transcription in endothelial cells, while IL-10 protein levels were elevated in RA FLS albeit to a lower extent than inflammatory mediators. Interestingly, RA FLS remodeled by Syntenin-1 or LPS/IFNγ mutually enhanced GLUT1, HK2, PFK2, and HIF1α transcription [41]. GLUT1 and HK2 transcriptional upregulation in LPS/IFNγ reprogrammed RA FLS was suppressed by 2-DG, although HIF1α levels were also negated by IACS, suggesting its involvement in oxidative stress [41]. The ability of Syntenin-1 to potentiate mitoATP alongside AMPK in RA FLS contrasted with RA fibroblasts differentiated by LPS/IFNγ or R837, where AMPK levels were unchanged [41, 42]. However, distinct from Syntenin-1 or R837 remodeled RA FLS, those reconfigured by LPS/IFNγ displayed citrate accumulation that was resolved by 2-DG and IACS therapy [41, 42]. The inflammatory profile uncovered in Syntenin-1, R837, and TNF-remodeled RA FLS were commonly abrogated by HIF1αi, while cMYCi only disrupted R837 differentiated RA FLS [42, 43]. Whereas TLR reprogramming in RA FLS is orchestrated by glycolytic activity, Syntenin-1-driven metabolic profile is dominated by oxidative stress leading to mitochondrial dynamic change through Mitofusin-2 and DRP1.

Interestingly, Syntenin-1, LPS/IFNγ, and IL-6/IFNγ promote RA FLS migration which can be impaired by SDC-1 Ab and mTOR1i (Syntenin-1 activated), glucose uptake blockade (LPS/IFNγ stimulated) or Tofacitinab therapy (IL-6/IFNγ signaling) respectively [41, 44]. Contrasting IL-6/IFNγ remodeled RA FLS, those reprogrammed by Syntenin-1 did not display STAT1/3 activation, however, both showed modest glycolytic activity facilitated through HK2 transcription [44].

Endothelial cells, RA FLS, or RA explants exposed to Syntenin-1, exhibited an expansion in VEGF/VEGFR and JAG1/Notch1 gene signature. In RA FLS and endothelial cell cocultures, IL-6 was shown to be responsible for VEGF production [45, 46]. Moreover, IL-6R Ab impaired the synergistic effect of IL-6, IL-1β, and TNF on VEGF production from RA FLS, while the blockade of IL-1β or TNF was ineffective on this manifestation [46, 47]. These findings indicate that escalated IL-6 levels together with TNF and IL-1β detected in Syntenin-1 reprogrammed endothelial cells and RA FLS may contribute to the identified proangiogenic gene signature.

In RA explants, HIF1α signaling can widely influence Syntenin-1 mediated inflammatory and pro-angiogenic mediators as well as RAPTOR activity. The inflammatory landscape of Syntenin-1 in endothelial cells and RA ST explants are similarly intercepted by mTORi or HIF1αi. While RA MΦ and Th1 cell reconfiguration by Syntenin-1 are mainly influenced by mTOR activation [14], RA FLS-mediated inflammation is exclusively modulated by HIF1α signaling in part due to its enriched frequency [26]. Ultimately, the Syntenin-1 arthritic mice portray the involvement of $F480^{+}iNOS^{hi}$ $Arginase^{lo}$ MΦs [14], $Vimentin^{+}$ fibroblasts, and VWF^{+}endothelial cells in advancing joint inflammation, angiogenesis, and hypermetabolic activity that can be counteracted by SDC-1 deficiency. In line with these findings, CIA joint inflammation, vascularization, and immunometabolism were mitigated in $SDC\text{-}1^{-/-}$ mice via intercepting the transcription of IL-6, DLL1/DLL4/JAG2/Notch1, and GLUT1 or mTOR respectively [18]. In conclusion, the Syntenin-1/SDC1 pathway is integral for RA progression due to its influence on various cell types that manipulate joint inflammation and metabolic malfunction.

DATA AVAILABILITY

All data generated or analyzed during this study are included in this paper and its supplementary information files.

REFERENCES

1. Boukerche H, Su ZZ, Prevot C, Sarkar D, Fisher PB. mda-9/Syntenin promotes metastasis in human melanoma cells by activating c-Src. Proc Natl Acad Sci USA. 2008;105:15914–9.

2. Boukerche H, Aissaoui H, Prevost C, Hirbec H, Das SK, Su ZZ, et al. Src kinase activation is mandatory for MDA-9/syntenin-mediated activation of nuclear factor-kappaB. Oncogene. 2010;29:3054–66.
3. Kang BS, Cooper DR, Jelen F, Devedjiev Y, Derewenda U, Dauter Z, et al. PDZ tandem of human syntenin: crystal structure and functional properties. Structure. 2003;11:459–68.
4. Latysheva N, Muratov G, Rajesh S, Padgett M, Hotchin NA, Overduin M, et al. Syntenin-1 is a new component of tetraspanin-enriched microdomains: mechanisms and consequences of the interaction of syntenin-1 with CD63. Mol Cell Biol. 2006;26:7707–18.
5. Grembecka J, Cierpicki T, Devedjiev Y, Derewenda U, Kang BS, Bushweller JH, et al. The binding of the PDZ tandem of syntenin to target proteins. Biochemistry. 2006;45:3674–83.
6. Luo P, Yang X, Huang S, Feng S, Ou Z. Syntenin overexpression in human lung cancer tissue and serum is associated with poor prognosis. BMC Cancer. 2020;20:159.
7. Das SK, Guo C, Pradhan AK, Bhoopathi P, Talukdar S, Shen XN, et al. Knockout of MDA-9/Syntenin (SDCBP) expression in the microenvironment dampens tumor-supporting inflammation and inhibits melanoma metastasis. Oncotarget. 2016;7:46848–61.
8. Holli K, Hietanen P, Saaristo R, Huhtala H, Hakama M, Joensuu H. Radiotherapy after segmental resection of breast cancer with favorable prognostic features: 12-year follow-up results of a randomized trial. J Clin Oncol. 2009;27:927–32.
9. Nault JC, Guyot E, Laguillier C, Chevret S, Ganne-Carrie N, N'Kontchou G, et al. Serum proteoglycans as prognostic biomarkers of hepatocellular carcinoma in patients with alcoholic cirrhosis. Cancer Epidemiol Biomarkers Prev. 2013;22:1343–52.
10. Wiksten JP, Lundin J, Nordling S, Lundin M, Kokkola A, von Boguslawski K, et al. Epithelial and stromal syndecan-1 expression as predictor of outcome in patients with gastric cancer. Int J Cancer. 2001;95:1–6.
11. Binder Gallimidi A, Nussbaum G, Hermano E, Weizman B, Meirovitz A, Vlodavsky I, et al. Syndecan-1 deficiency promotes tumor growth in a murine model of colitis-induced colon carcinoma. PLoS One. 2017;12:e0174343.
12. Jaiswal AK, Sadasivam M, Archer NK, Miller RJ, Dillen CA, Ravipati A, et al. Syndecan-1 Regulates Psoriasiform Dermatitis by Controlling Homeostasis of IL-17-Producing gammadelta T Cells. J Immunol. 2018;201:1651–61.
13. Jaiswal AK, Sadasivam M, Aja S, Hamad ARA. Lack of Syndecan-1 produces significant alterations in whole-body composition, metabolism and glucose homeostasis in mice. World J Diabetes. 2020;11:126–36.
14. Meyer A, Sienes RE, Nijim W, Zanotti B, Umar S, Volin MV et al. Syntenin-1-mediated arthritogenicity is advanced by reprogramming RA metabolic macrophages and Th1 cells. Ann Rheum Dis. 2023.
15. Van Raemdonck K, Umar S, Palasiewicz K, Volin MV, Elshabrawy HA, Romay B et al. IL-34 reprograms glycolytic and osteoclastic RA macrophages via Syndecan-1 and M-CSFR. Arthritis Rheumatol. 2021.
16. Lewis MJ, Barnes MR, Blighe K, Goldmann K, Rana S, Hackney JA, et al. Molecular Portraits of Early Rheumatoid Arthritis Identify Clinical and Treatment Response Phenotypes. Cell reports. 2019;28:2455–2470 e2455.
17. Barre PE, Redini F, Boumediene K, Vielpeau C, Pujol JP. Semiquantitative reverse transcription-polymerase chain reaction analysis of syndecan-1 and -4 messages in cartilage and cultured chondrocytes from osteoarthritic joints. Osteoarthritis Cartilage. 2000;8:34–43.
18. Meyer A, Sienes R, Zanotti B, van Raemdonck K, Palasiewicz K, Mass DP, et al. Dysregulation of IL-34 ligation to SDC-1 mitigates collagen-induced arthritis. Cell Mol Immunol. 2022;19:1070–2.
19. Pickens SR, Chamberlain ND, Volin MV, Pope RM, Mandelin AM 2nd, Shahrara S. Characterization of CCL19 and CCL21 in rheumatoid arthritis. Arthritis Rheum. 2011;63:914–22.
20. Pickens SR, Chamberlain ND, Volin MV, Pope RM, Talarico NE, Mandelin AM 2nd, et al. Characterization of interleukin-7 and interleukin-7 receptor in the pathogenesis of rheumatoid arthritis. Arthritis Rheum. 2011;63:2884–93.
21. Chamberlain ND, Vila OM, Volin MV, Volkov S, Pope RM, Swedler W, et al. TLR5, a novel and unidentified inflammatory mediator in rheumatoid arthritis that correlates with disease activity score and joint TNF-alpha levels. J Immunol. 2012;189:475–83.
22. Elshabrawy HA, Volin MV, Essani AB, Chen Z, McInnes IB, Van Raemdonck K, et al. IL-11 facilitates a novel connection between RA joint fibroblasts and endothelial cells. Angiogenesis. 2018;21:215–28.
23. Chen Z, Kim SJ, Essani AB, Volin MV, Vila OM, Swedler W, et al. Characterising the expression and function of CCL28 and its corresponding receptor, CCR10, in RA pathogenesis. Ann Rheum Dis. 2015;74:1898–906.
24. Kim SJ, Chen Z, Chamberlain ND, Volin MV, Swedler W, Volkov S, et al. Angiogenesis in Rheumatoid Arthritis Is Fostered Directly by Toll-like Receptor 5 Ligation and Indirectly Through Interleukin-17 Induction. Arthritis Rheum. 2013;65:2024–36.
25. Humby F, Lewis M, Ramamoorthi N, Hackney JA, Barnes MR, Bombardieri M, et al. Synovial cellular and molecular signatures stratify clinical response to csDMARD therapy and predict radiographic progression in early rheumatoid arthritis patients. Ann Rheum Dis. 2019;78:761–72.
26. Wei K, Korsunsky I, Marshall JL, Gao A, Watts GFM, Major T, et al. Notch signalling drives synovial fibroblast identity and arthritis pathology. Nature. 2020;582:259–64.
27. Wang J, Conlon D, Rivellese F, Nerviani A, Lewis MJ, Housley W, et al. Synovial Inflammatory Pathways Characterize Anti-TNF-Responsive Rheumatoid Arthritis Patients. Arthritis Rheumatol. 2022;74:1916–27.
28. van Riel PL, Renskers L. The Disease Activity Score (DAS) and the Disease Activity Score using 28 joint counts (DAS28) in the management of rheumatoid arthritis. Clin Exp Rheumatol. 2016;34:S40–S44.
29. Rivellese F, Surace AEA, Goldmann K, Sciacca E, Cubuk C, Giorli G, et al. Rituximab versus tocilizumab in rheumatoid arthritis: synovial biopsy-based biomarker analysis of the phase 4 R4RA randomized trial. Nat Med. 2022;28:1256–68.
30. Alexander CM, Reichsman F, Hinkes MT, Lincecum J, Becker KA, Cumberledge S, et al. Syndecan-1 is required for Wnt-1-induced mammary tumorigenesis in mice. Nat Genet. 2000;25:329–32.
31. Van Raemdonck K, Umar S, Palasiewicz K, Meyer A, Volin MV, Chang HJ, et al. Metabolic reprogramming of macrophages instigates CCL21-induced arthritis. Immunol Cell Biol. 2022;100:127–35.
32. Umar S, Palasiewicz K, Van Raemdonck K, Volin MV, Romay B, Amin MA, et al. IRAK4 inhibition: a promising strategy for treating RA joint inflammation and bone erosion. Cell Mol Immunol. 2021;18:2199–210.
33. Salminen A, Kaarniranta K, Kauppinen A. AMPK and HIF signaling pathways regulate both longevity and cancer growth: the good news and the bad news about survival mechanisms. Biogerontology. 2016;17:655–80.
34. Li H, Satriano J, Thomas JL, Miyamoto S, Sharma K, Pastor-Soler NM, et al. Interactions between HIF-1alpha and AMPK in the regulation of cellular hypoxia adaptation in chronic kidney disease. Am J Physiol Renal Physiol. 2015;309:F414–428.
35. Hwang AB, Ryu EA, Artan M, Chang HW, Kabir MH, Nam HJ, et al. Feedback regulation via AMPK and HIF-1 mediates ROS-dependent longevity in Caenorhabditis elegans. Proc Natl Acad Sci USA. 2014;111:E4458–4467.
36. Tae N, Lee S, Kim O, Park J, Na S, Lee JH. Syntenin promotes VEGF-induced VEGFR2 endocytosis and angiogenesis by increasing ephrin-B2 function in endothelial cells. Oncotarget. 2017;8:38886–901.
37. Das SK, Bhutia SK, Azab B, Kegelman TP, Peachy L, Santhekadur PK, et al. MDA-9/syntenin and IGFBP-2 promote angiogenesis in human melanoma. Cancer Res. 2013;73:844–54.
38. Javadi J, Heidari-Hamedani G, Schmalzl A, Szatmari T, Metintas M, Aspenstrom P et al. Syndecan-1 Overexpressing Mesothelioma Cells Inhibit Proliferation, Wound Healing, and Tube Formation of Endothelial Cells. Cancers (Basel). 2021; 13.
39. Xiao W, Oldham WM, Priolo C, Pandey AK, Loscalzo J. Immunometabolic Endothelial Phenotypes: Integrating Inflammation and Glucose Metabolism. Circ Res. 2021;129:9–29.
40. Wong BW, Marsch E, Treps L, Baes M, Carmeliet P. Endothelial cell metabolism in health and disease: impact of hypoxia. EMBO J. 2017;36:2187–203.
41. Umar S, Palasiewicz K, Volin MV, Romay B, Rahat R, Tetali C et al. Metabolic regulation of RA macrophages is distinct from RA fibroblasts and blockade of glycolysis alleviates inflammatory phenotype in both cell types. Cell Mol Life Sci. 2021.
42. Umar S, Palasiewicz K, Volin MV, Zanotti B, Al-Awqati M, Sweiss N et al. IRAK4 inhibitor mitigates joint inflammation by rebalancing metabolism malfunction in RA macrophages and fibroblasts. Life Sci. 2021; 120114.
43. Koedderitzsch K, Zezina E, Li L, Herrmann M, Biesemann N. TNF induces glycolytic shift in fibroblast like synoviocytes via GLUT1 and HIF1A. Sci Rep. 2021;11:19385.
44. Palasiewicz K, Umar S, Romay B, Zomorrodi RK, Shahrara S Tofacitinib therapy intercepts macrophage metabolic reprogramming instigated by SARS-CoV-2 Spike protein. Eur J Immunol. 2021.
45. Kayakabe K, Kuroiwa T, Sakurai N, Ikeuchi H, Kadiombo AT, Sakairi T, et al. Interleukin-6 promotes destabilized angiogenesis by modulating angiopoietin expression in rheumatoid arthritis. Rheumatology (Oxford). 2012;51:1571–9.
46. Elshabrawy HA, Chen Z, Volin MV, Ravella S, Virupannavar S, Shahrara S. The pathogenic role of angiogenesis in rheumatoid arthritis. Angiogenesis. 2015;18:433–48.
47. Nakahara H, Song J, Sugimoto M, Hagihara K, Kishimoto T, Yoshizaki K, et al. Anti-interleukin-6 receptor antibody therapy reduces vascular endothelial growth factor production in rheumatoid arthritis. Arthritis Rheum. 2003;48:1521–9.

ACKNOWLEDGEMENTS

The authors would like to thank Dr. Sadiq Umar for assistance with RA FLS culture and Ms. Pei-Yu Wu for her excellent scientific advice, and the Fluorescent

Immunohistochemistry Midwestern University Core Facility, Downers Grove, IL for analyzing the fluorescent stainings. Moreover, we would like to acknowledge Dr. Caroline Alexander (University of Wisconsin–Madison) for generously providing us with SDC-1$^{-/-}$ mice [30]. Schematic figures were illustrated by biorender.com.

AUTHOR CONTRIBUTIONS

All authors were involved in drafting the article or revising it critically for important intellectual content, and all authors approved the final version to be published. Dr. Shahrara had full access to all of the data in the study and takes responsibility for the integrity of the data and the accuracy of the data analysis. Study conception and design: AM, SZ, SS Acquisition of data: AM, SZ, WN, AB, VP, BZ, MV, ML, CP, SS Analysis and interpretation of data: AM, SZ, WN, AB, VP, BZ, MV, MAA, ML, CP, IM, SA, JAK, NS, SS Providing crucial reagents: MAA, SA, JAK, NS.

FUNDING

This work was supported in part by awards from the Department of Veteran's Affairs MERIT Award BX002286, CX002565, IK6BX006474, the National Institutes of Health NIH R01 AI167155, NIH R41 AI147697, and the Innovative Research Award from the Rheumatology Research Foundation (RRF, no number assigned).

RESEARCH ETHICS APPROVAL

RA patients were collected according to the protocol approved by the University of Illinois at Chicago Institutional Ethics Review Board (protocol# 2021-1494). All animal studies were approved by the University of Illinois at Chicago Animal Care and Use Committee (protocol# 22-008). To ensure a robust and unbiased experimental design, samples were obtained from RA patients or mice of both genders. Mice used within the same experimental group were age and sex-matched. Rigor and reproducibility were maintained through well-powered studies and multiple distinct approaches to confirm the results. Power was calculated using parameters of α=0.05, and power=90%.

COMPETING INTERESTS

The authors declare no competing interests.

ADDITIONAL INFORMATION

Supplementary information The online version contains supplementary material available at https://doi.org/10.1038/s41423-023-01108-8.

Correspondence and requests for materials should be addressed to Shiva Shahrara.

Reprints and permission information is available at http://www.nature.com/reprints